Modelling GNSS-observed seasonal velocity changes of the Ross Ice Shelf, Antarctica, using the Ice-sheet and Sea-level System Model (ISSM)

Francesca Baldacchino[1,2], Nicholas R. Golledge[1], Mathieu Morlighem[3], Huw Horgan[1,4,5], Alanna V. Alevropoulos-Borrill[1], Alena Malyarenko[6,1], Alexandra Gossart[1], Daniel P. Lowry[7], and Laurine van Haastrecht[1]

[1]Te Puna Pātiotio | Antarctic Research Centre, Te Herenga-Waka, Victoria University of Wellington, Aotearoa | New Zealand
[2]Institute of Geodesy, Working Group Remote Sensing and Photogrammetry, Graz University of Technology, Austria
[3]Department of Earth Sciences, Dartmouth College, Hanover, NH 03755, USA
[4]Laboratory of Hydraulics, Hydrology and Glaciology (VAW), ETH Zurich, Zurich, Switzerland
[5]Swiss Federal Institute for Forest, Snow and Landscape Research (WSL), Birmensdorf, Switzerland
[6]School of Earth and Environment | Te Kura Aronukurangi, University of Canterbury | Te Whare Wānanga o Waitaha, Ōtautahi | Christchurch
[7]Department of Surface Geosciences, GNS Science, Lower Hutt, New Zealand

Correspondence: Francesca Baldacchino (francesca.baldacchino@tugraz.at)

Abstract. ~~Recently, seasonal changes in sea ice cover have been found to elevate basal melt rates~~ Recent observations show that the ice flow of the Ross Ice Shelf (RIS) ~~calving front at sensitive regions. Melting at these sensitive regions has been found to impact ice sheet mass balance. However, the influence of these seasonally elevated basal melt rates on RIS flow variability is not yet fully understood. This paper aims to explore whether seasonal perturbations in basal melt rates of the RIS can explain~~ has a clear seasonal signal. The drivers of these seasonal fluctuations in ice speed are still poorly understood. We present here three new velocity datasets from GNSS stations on the RIS collected between early 2020 and late 2021. It has previously been suggested that changes in sea surface height (SSH) was the main driver of these variations, requiring the grounding lines to migrate significantly further upstream than the point of hydrostatic equilibrium. Our new dataset, however, displays clear intra-annual ~~variations in ice flow measured by GNSS at four sites across the ice shelf. We~~ velocity variability at the three sites, with two distinct peaks observed in austral summer and austral winter, which is not consistent with the yearly cycle of SSH. Here, we investigate the potential role of basal melting, and whether it would be capable of causing the observed variability in ice speed. In order to determine where changes in melt would have the largest influence on ice velocity, we use the automatic differentiation tool in the Ice-sheet and Sea-level System Model (ISSM) to identify ~~regions of the RIS where changes in basal melt affect ice velocities~~ the areas where the ice flow speed recorded at the GNSS sites are most sensitive to changes in basal melting. Next, we seasonally perturb Massachusetts Institute of Technology general circulation (MITgcm) basal melt rates in ISSM at these ~~sensitive regions to try and replicate~~ identified sensitive regions until we reproduce similar velocity variability to the GNSS ice flow observations. ~~The GNSS observations display clear~~ Using this approach, we can reproduce the intra-annual ~~velocity variability at the four sites, with two distinct peaks observed in austral summer and austral winter. We can replicate this intra-annual~~ velocity variation for GNSS sites near the calving front ~~by seasonally perturbing the basal melt rates at the~~

20 ~~identified sensitive regions of the ice shelf. We argue that the perturbed seasonal basal melt variability at sensitive regions along the calving front is a realistic scenario for the RIS. Thus,~~ but only when high melt rates are applied. However, this approach fails for GNSS sites located far from the calving front and we suggest that ~~the GNSS-recorded~~ a combination of external forcings and internal mechanics may be needed to reproduce the observed intra-annual ~~velocity variations along the calving front could be partly driven by seasonal changes in basal melting today. We also try to replicate intra-annual~~ velocity ~~variability observed at~~

25 ~~the Siple Coast by seasonally perturbing basal melt rates at sensitive regions there. However, we are unable to replicate similar magnitudes of velocity variations to the GNSS measurements and suspect that the perturbed seasonal basal melt variability is unrealistic, with no observations of seasonally high basal melt rates at the Siple Coast grounding lines or pinning points. Thus, seasonal changes in basal melt cannot explain the observed intra-annual velocity variability at all the GNSS sites, and further work is needed. Our~~ variation at these sites. While this study does not bring a definitive answer to the question of what the

30 drivers of seasonality in ice flow are, this study shows that seasonal basal melt rates could explain the GNSS velocity variability on an seasonal timescale for two of the four GNSS sites. Additionally, our sensitivity maps highlight regions of the ice shelf where changes in basal melt most influence velocities ~~,~~ and are a valuable addition to fieldwork campaigns and modelling studies.

1 Introduction

35 The Antarctic Ice Sheet (AIS) contains the vast majority of Earth's freshwater and has the potential to raise global sea levels by 58 m (Mottram et al., 2019; Schlegel et al., 2018; Dirscherl et al., 2020). Over recent decades, the AIS has been losing mass at an accelerating rate due to the warming of the atmosphere and ocean (Pattyn et al., 2018; Shepherd et al., 2012, 2018; Jenkins et al., 2018; Rignot et al., 2019; Lipscomb et al., 2021). Ocean-forced basal melting and calving drive the largest mass losses on the AIS (Pattyn et al., 2018; Rignot et al., 2019; Adusumilli et al., 2020; Joughin et al., 2014). Floating ice

40 shelves, in particular, provide buttressing to grounded ice and thus are vital for controlling AIS mass loss (Schoof, 2007; Gudmundsson, 2013; Dinniman et al., 2016; Joughin et al., 2013; Pattyn and Durand, 2013). Ocean-forced basal melting thins ice shelves, reducing their buttressing ability of the grounded ice, which in turn increases ice discharge and grounding line retreat (Depoorter et al., 2013; Joughin et al., 2013; Jenkins et al., 2018; Greene et al., 2022; Smith et al., 2020; Gudmundsson et al., 2019).

45 The Ross Ice Shelf (RIS) is Antarctica's largest ice shelf by area and is approximately in balance (Moholdt et al., 2014; Rignot et al., 2013; Depoorter et al., 2013)~~with average basal melt rates of approximately 0.1 m/a (Klein et al., 2020; Das et al., 2020). These basal melt rates are relatively low due to the cold dense water masses formed on the continental shelf blocking the sub-ice-shelf ocean cavity from warm Circumpolar Deep Water (CDW) intrusions (Moholdt et al., 2014; Stevens et al., 2020; Adusumilli et~~ ~~. However, basal melt rates of the RIS vary spatially as they are driven by subsurface inflows of cold High Salinity Shelf Water~~

50 ~~(HSSW) near the grounding lines and seasonal inflows of summer-warmed Antarctic Surface Water (AASW) at the calving front (Stewart et al., 2019; Stevens et al., 2020; Klein et al., 2020; Jendersie et al., 2018; Dinniman et al., 2016; Adusumilli et al., 2020). Recently, high basal melt rates have been observed at the calving front near Ross Island due to~~ Currently, there is limited

understanding of the influence of seasonal oceanic and atmospheric variability on the flow dynamics of the ~~seasonal inflow of summer-warmed AASW from the adjacent Ross Sea Polynya downwelling into the ice shelf cavity (Stewart et al., 2019; Malyarenko et al.,~~

55 ~~. Ross Island has been identified as a sensitive region where changes in ice thickness can drive changes in ice shelf dynamics and mass balance (Reese et al., 2018; Gudmundsson et al., 2019; Fürst et al., 2016; Baldacchino et al., 2022). With predicted surface warming and declines in summer sea ice, these high basal melt rates along the calving front are projected to increase (Stewart et al., 2019; Dinniman et al., 2018; Schodlok et al., 2016; Smith Jr. et al., 2014). Additionally, high basal melt rates may occur in the future due to changes in the primary modes of basal melting of the RIS, such as increases in the amount~~

60 ~~of Modified Circumpolar Deep Water (mCDW) heat flux flowing onto the continental shelf and reducing the rate of sea ice formation (Tinto et al., 2019; Reddy et al., 2007). mCDW is formed by CDW flowing onto the continental shelf of the Ross Sea and mixing with the AASW and HSSW (Dinniman et al., 2018; Smith Jr. et al., 2014).~~

~~Understanding the flow variability of the RIS is essential for monitoring mass balance changes~~RIS. It is important to understand the impact of this seasonality on ice shelf flow as this may provide further understanding of the processes controlling

65 ice shelf mass balance over longer timescales (Mosbeux et al., 2023; Dutrieux et al., 2014; Paolo et al., 2018; Jenkins et al., 2018) . Ice shelves flow by gravity-driven horizontal spreading with resistance to flow provided by shear at bay walls and pinning points ~~(Hulbe et al., 2013; Cuffey and Paterson, 2010)~~(Thomas, 1979; Hulbe et al., 2013; Cuffey and Paterson, 2010). Changes in ice shelf dynamics, geometry, and mass can lead to changes in velocity on floating and grounded ice (Fürst et al., 2016; Reese et al., 2018; Gudmundsson et al., 2019; Mosbeux et al., 2023). The RIS has typical flow speeds of several hundred meters per

70 year, with the active Siple Coast Ice Streams and Byrd Glacier displaying velocities of > 300 m/a (Figure 1). The ice shelf front exhibits the fastest flow rates of 800 - 1200 m/a (Figure 1) (Rignot et al., 2017). The Siple Coast Ice Streams and Transantarctic Mountain outlet glaciers are the main conduits of ice discharging into the RIS from the West Antarctic Ice Sheet (WAIS) and East Antarctic Ice Sheet (EAIS), respectively (Shabtaie and Bentley, 1987; Bennett, 2003; Bindschadler et al., 2003; Catania et al., 2012b) (Figure 1). ~~The Siple Coast Ice Streams are underlain by deformable till that is water-saturated~~

75 ~~(Kamb, 1991; MacAyeal, 1992; Joughin et al., 2004) and basal friction at their beds and along the lateral margins are the primary forces resisting flow (Ranganathan et al., 2021). The Kamb Ice Stream (KIS) has been inactive for the last 160 years (Retzlaff and Bentley, 1993; Thomas et al., 2013), and the Whillans and Mercer ice streams are slowing down and could reach stagnation in the next 50 years (Thomas et al., 2013). In the Transantarctic Mountains, flow of the Byrd Glacier is driven by high driving stresses modulated by changes in subglacial hydrology (Whillans et al., 1989; Van Der Veen et al., 2014; Stearns. et al., 2008)~~

80 ~~.~~

~~Currently, the influence of seasonal oceanic and atmospheric variability on the flow dynamics of the RIS is unknown. Previous studies have suggested that RIS velocities may be modulated at seasonal to interannual timescales by basal melting at the calving front (Stewart et al., 2019; Tinto et al., 2019). It is important to understand the impact of this seasonality on ice shelf flow as this may provide further understanding of the processes controlling ice shelf mass balance over longer timescales~~

85 ~~(Mosbeux et al., 2023; Dutrieux et al., 2014; Paolo et al., 2018; Jenkins et al., 2018).~~ Global Navigation Satellite System (GNSS) receivers ~~near-continuously record~~ can record near-continuously at high temporal resolution throughout the ~~winter and summer seasons and~~ year and thus have the ~~unique~~ ability to measure seasonal variations in ice velocities (Brunt, 2008; King et al.,

2011; Brunt and Macayeal, 2014). Typically, GNSS receivers are employed to measure ice velocities over 1–3 months in the austral summer and to highlight short timescale processes such as tidal ~~fluctuations within one season. However, previous~~

90 ~~studies have observed inter-annual~~ variability (e.g. Bindschadler et al., 2003). In this study, we present three new long-duration (12 - 24 months) GNSS datasets of intra-annual ice velocity variations on the RIS. We explore three new sites: the shear margin (Site 1) and the calving front (Site 2) near the Ross Island pinning point, and the KIS grounding zone (Site 4; Figure 1). Additionally, the GNSS dataset previously reported in Mosbeux et al. (2023); Klein et al. (2020) (referred to as DR10) are explored in this study.

95 Previous multi-season GNSS observations on the RIS have noted intra-annual (monthly to seasonal) velocity variations~~using GNSS instruments deployed on the RIS over multiple seasons (Klein et al., 2020; Mosbeux et al., 2023). Klein et al. (2020) use~~, with one distinct peak per year in the austral winter (Klein et al., 2020; Mosbeux et al., 2023). Two mechanisms have been proposed to explain this intra-annual variability. Firstly, Klein et al. (2020) investigated the impact of a seasonal cycle of spatially varying basal melt rates on the RIS using ice sheet modelling~~to conclude that these~~. Klein et al. (2020) used

100 monthly basal melt rates from the ocean model described by Tinto et al. (2019). This ocean model was developed using a repeated annual cycle of forcing for the period 2001-2002 and therefore does not account for known inter-annual ~~velocity variations~~ variability in atmospheric, oceanic and sea-ice conditions in the Ross Sea (Klein et al., 2020). Klein et al. (2020) concluded that the GNSS-observed intra-annual velocity variations on the RIS are not driven by seasonal basal melt rates and that some other seasonal forcing must be ~~driving the velocity variations for one site on the RIS~~dominant. They found

105 that their modelled variability of ice velocity was much smaller than their GNSS observations (Klein et al., 2020). More recently, Mosbeux et al. (2023) used ~~a viscoelastic model, concluding that the observed intra-annual velocity variations on the RIS are driven by seasonal variations in Sea Surface Height~~ ice sheet modelling to investigate whether the seasonal variability of sea surface height (SSH) ~~. Mosbeux et al. (2023) were able to reproduce the GNSS measured~~ modifies ice velocity through a combination of sea surface tilt and changing basal stresses at the grounding zone. Mosbeux et al. (2023) successfully

110 reproduced the GNSS-observed intra-annual velocity variability at their GNSS sites if a sufficiently large cycle of SSH-induced basal shear stress change near the grounding line was parameterized in their ice sheet model~~(Mosbeux et al., 2023).~~

~~This paper aims to explore whether perturbations in basal melt rates on the RIS can explain the~~. They found that, in order to capture the observed change in flow speed, they had to allow for the model grounding line to retreat significantly further upstream than what hydrostatic equilibrium would dictate, using a parameterization of viscoelastic processes (Mosbeux et al., 2023)

115 . Furthermore, Mosbeux et al. (2023) modelled SSH velocity variability displays one distinct peak per year, in contrast to our GNSS observations, which display two distinct peaks per year. This suggests that seasonal variability in SSH is unlikely to be the only forcing that explains the observed variability in velocities at our GNSS sites. We therefore turn again to the potential role of basal melt as it is known to be an important control on ice shelf dynamics.

The RIS basal melt rates are relatively low due to the cold dense water masses formed on the continental shelf blocking the

120 sub-ice-shelf ocean cavity from warm Circumpolar Deep Water (CDW) intrusions (Moholdt et al., 2014; Stevens et al., 2020; Adusumilli et . However, basal melt rates of the RIS vary spatially as they are driven by subsurface inflows of cold High Salinity Shelf Water (HSSW) that reach the grounding zone and seasonal inflows of summer-warmed Antarctic Surface Water (AASW) at the

calving front (Stewart et al., 2019; Stevens et al., 2020; Klein et al., 2020; Jendersie et al., 2018; Dinniman et al., 2016; Adusumilli et al., ?. Recently, high basal melt rates have been observed at the calving front near Ross Island due to the seasonal inflow of summer-warmed AASW from the adjacent Ross Sea Polynya downwelling into the ice shelf cavity (Stewart et al., 2019; Malyarenko et al., ?. Previous studies have suggested that RIS velocities may be modulated at seasonal to intra-annual timescales by basal melting at the calving front (Stewart et al., 2019; Tinto et al., 2019). Ross Island has been identified as a sensitive region where changes in ice thickness can drive changes in ice shelf dynamics and mass balance (Reese et al., 2018; Gudmundsson et al., 2019; Fürst et al., 2016; ?. With predicted surface warming and declines in summer sea ice, these high basal melt rates along the calving front are projected to increase (Stewart et al., 2019; Dinniman et al., 2018; Schodlok et al., 2016; Smith Jr. et al., 2014). Additionally, high basal melt rates may occur in the future due to changes in the primary modes of basal melting of the RIS. Such changes include increases in the amount of Modified Circumpolar Deep Water (mCDW) heat flux flowing onto the continental shelf and reducing the rate of sea ice formation (Tinto et al., 2019; Reddy et al., 2007). mCDW is formed by CDW flowing onto the continental shelf of the Ross Sea and mixing with the AASW and HSSW (Dinniman et al., 2018; Smith Jr. et al., 2014).

In this study, we aim to investigate whether perturbations in basal melt rates can reproduce the observed intra-annual vari-ations in ice velocities at four sites across the RIS. ~~This paper presents three new long-duration (12 - 24 months) GNSS measurements of~~ Klein et al. (2020) concluded that basal melt is not driving the observed intra-annual ~~ice velocity variations~~ velocity variability on the RIS. ~~We explore four sites: the shear margin near Ross Island (Site 1), the calving front near Coulman High (Site 2), a mid-shelf region (Site 3) , and the KIS grounding zone (Site 4; Figure 1). The GNSS receivers display clear intra-annual velocity variability, with~~ , but 'basal melting can explain some of the observed seasonality in ice flow'. Therefore, we aim to further test this hypothesis by (1) presenting three new GNSS datasets which display two distinct velocity peaks ~~each year : one in the austral summer and one in austral winter~~ per year (a different intra-annual velocity variability to those presented in Klein et al. (2020); Mosbeux et al. (2023)) and (2) using a novel approach of combining the Automatic Differentiation tool in ISSM and perturbed weekly MITgcm basal melt rates to enable us to identify whether seasonal changes in basal melt rates at identified sensitive regions can reproduce the observed intra-annual velocity variability. Baldacchino et al. (2022) showed that RIS mass balance is sensitive to changes in basal melt at specific locations. ~~We apply here~~ Here we apply a similar approach to identify the regions where flow speed at GNSS locations is most sensitive to melt ~~, and we further explore if changes in basal melt at these locations can explain the observed velocity time series~~. We use multiple basal melt peaks as the basis for our phasing of the basal melt forcing, and apply perturbations on this forcing until we reproduce a similar velocity variability to the GNSS observations. Therefore, our study serves as a proof of concept, motivated by Klein et al. (2020) 'other as-yet-unidentified seasonal processes' driving the observed velocity variations on the RIS.

2 Locations and Methods

2.1 Global Navigation Satellite Systems locations

~~Figure 1 highlights the locations of the four~~ We present results from three new GNSS sites (Sites 1, 2 and 4), and a previously reported GNSS site (Site 3)(Mosbeux et al., 2023; Klein et al., 2020) on the Ross Ice Shelf ~~GNSS sites explored in this paper.~~

Firstly, GNSS (Figure 1). The three new GNSS units were installed during field season 2019/2020 and the data was downloaded in December 2021 (Sites 1, 2, and 4 in Figure 1). These GNSS units were battery-powered and deployed on the RIS for multiple field seasons to provide a long-term continuous dataset that can observe intra-annual velocity variations. The GNSS unit at Site 3 is the same as that in Klein et al. (2020) and is described in more detail in their study (referred to as DR10) (Figure 1).

Site 1 is located close to Ross Island, which is a major pinning point making it a sensitive region where changes in ice thickness are expected to influence the flow speed and mass balance of the entire ice shelf (Gudmundsson et al., 2019; Fürst et al., 2016; Baldacchino et al., 2022; Reese et al., 2018) (Figure 1). Pinning points such as Ross Island provide resistance to ice shelf flow by modifying the balance of forces within the floating ice (Still et al., 2019; Cuffey and Paterson, 2010). This modification of forces has an effect everywhere on the ice shelf due to the balance of forces in floating ice being non-local (Still et al., 2019; Cuffey and Paterson, 2010). High basal melt rates with a seasonal signal have been observed close to the Ross Island pinning point (Stewart et al., 2019). These basal melt rates may thin the ice, reduce the resistance of the pinning point and drive changes in ice shelf flow. Site 1 GNSS unit recorded every 30 seconds for 1 hour every 6 hours and has 80 days of data missing in July - October 2020, and 70 days in July - September 2021.

Site 2 is located at Coulman High close to the calving front ice front approximately 50 km from Ross Island and is likely to be influenced by seasonal changes in basal melting (Figure 1). High basal melt rates have been observed in this region due to and correlate with declines in sea ice cover and warming of the AASW during the austral summer (Stewart et al., 2019). Site 2 is located within the "passive" region of the ice shelf and thus this region can be removed without impacting the mass balance of the ice shelf (Fürst et al., 2016). However, thinning of this region or changes in the ice-front location (i.e., via iceberg calving) will alter the stress balance and velocities of the ice shelf (Gudmundsson et al., 2019; Klein et al., 2020). Site 2 GNSS unit recorded every 30 seconds over 24 hours and has 104 days of data missing in June - November 2020 and 30 days in July - August 2021.

Site 3 is located in the mid-shelf region of the RIS (200km from the calving front) and is the same site (referred to as DR10) also previously reported in Klein et al. (2020) and Mosbeux et al. (2023) (Figure 1). Ice flow in the central portion of the RIS is primarily extensional which leads to along-flow thinning (Das et al., 2020). There are no pinning points or ice rises within the vicinity of Site 3, and no observations of high basal or surface (Adusumilli et al., 2020) or surface (Agosta et al., 2019) melt rates here. The Site 3 GNSS unit recorded every 30 seconds over 24 hours for 1 year (2015 - 2016), with a few days dropped in the austral winter of 2016 (Klein et al., 2020).

Finally, Site 4 is located at the Kamb Ice Stream (KIS) grounding line (Figure 1). The KIS has been inactive for the last 160 years likely due to a change in subglacial hydrology (Retzlaff and Bentley, 1993; Thomas et al., 2013; Hulbe et al., 2016). The KIS used to flow at speeds of 350 m/a but presently flows at speeds of less than 5 m/a (Rignot et al., 2017) (Rignot et al., 2017; Ng and Conway, 2004). Studies have indicated that the KIS could reactivate this century due to its hydrological setting and the length of time it has been inactive (Bougamont et al., 2015; van der Wel et al., 2013).

2.2 Global Navigation Satellite Systems data and processing

Three of the GNSS units were installed during field seasons 2019/2020 and data was downloaded in December 2021 (Sites
190   1, 2, and Site 4 in Figure 1). These GNSS units were battery-powered and deployed on the RIS for multiple field seasons to
provide a long-term continuous dataset that can observe intra-annual velocity variations. Site 1 GNSS unit recorded every 30
seconds for 1 hour every 6 hours, while the Site 2 GNSS unit recorded every 30 seconds over 24 hours. Site 4 GNSS unit
recorded every 30 seconds and operated continuously, but was shifted approximately 2.7 km upstream in December 2020. The
GNSS unit at Site 3 is the same as that in Klein et al. (2020) and is described in more detail in their paper (referred to as DR10)
195   (Figure 1). Site 1 GNSS unit has 80 days of data missing in July - October 2020, and 70 days in July - September 2021, while
Site 2 GNSS unit has 104 days of data missing in June - November 2020 and 30 days in July - August 2021. The Site 3 GNSS
unit recorded every 30 seconds over 24 hours for 1 year (2015 - 2016), with a few days dropped in the austral winter of 2016
(Klein et al., 2020).

Modelled Ross Ice Shelf surface velocities after initialisation. The grounding line is marked in white. The GNSS sites are
200   shown: Site 1 (shear margin region), Site 2 (Coulman High region), Site 3 (mid-shelf region), and Site 4 (KIS grounding zone).
Locations discussed in this paper are also labelled. These include the Siple Coast Ice Streams: Mercer Ice Stream (MIS),
Whillans Ice Stream (WIS), Kamb Ice Stream (KIS), Bindschadler Ice Stream (BIS), and MacAyeal Ice Stream (MacIS). Byrd
Glacier (BG) and Ross Island are also labelled. In addition, the ice rises are labelled on the Siple Coast: CIR = Crary Ice Rise,
SIR = Steershead Ice Rise, SCIR = Shirase Coast Ice Rumples, and Roosevelt Island. The projection of this map and all others
205   presented is polar stereographic with a true scale at -71° (EPSG:3031).

2.2   Global Navigation Satellite Systems processing

GNSS data were processed using the Precise Point Positioning (PPP) methodology (Zumberge et al., 1997) (Zumberge et al., 1997; Tétreau
and Natural Resources Canada's Canadian Spatial Reference System Precise Point Positioning (CSRS-PPP) post-processing
service[1]. For the 30-second sampled continuous data (sites Sites 2, 3, and 4), data were divided into 3-hour segments and pro-
210   cessed statically to obtain a single position every 3 hours. For Site 1, which has a different sampling frequency, the data were
divided into 1-hour segments every 6 hours and a single position was obtained every 6 hours. Data processing was iterated
whereby the initial positions were updated with the first processing results and then reprocessed to obtain new position solu-
tions. The position solutions were then projected into polarstereographic coordinates (EPSG:3031) and then used to estimate
site velocity by weighted linear regression through x and y coordinates. The position weightings were provided by the reported
215   processing uncertainty. Regression gradients provided velocities in the x and y direction (v_x, v_y) with gradient uncertainties
propagated to provide uncertainties in velocity and direction. The linear regression of positions was estimated at every time
step (either 3 hourly or 6 hourly) over centered time windows of 8 weeks duration. This provides a low-noise time series with
a high spatial temporal fidelity (albeit smoothed) that shows the seasonal cycle in velocity without aliasing spring-neap tidal
velocity signals. The use of the 8-week window duration to estimate velocity means a stepwise increase in velocity would
220   appear as a smooth increase in velocity beginning 4-weeks earlier that otherwise rapid changes in velocity are smoothed over
an 8-week period. Other time window lengths were tested and the seasonal signal was seen to be largely independent of the

---

[1]https://webapp.csrs-scrs.nrcan-rncan.gc.ca/geod/tools-outils. Last accessed: 15.08.2023

length used. The resulting uncertainties were low with 99% of the 1σ velocity uncertainties less than 0.04 m/a for sites 1 and 3, less than 0.06 m/a for Site 2, and less than 0.01 m/a for Site 4. We present all velocities as both absolute velocity (Figure 2) and as the deviation from the initial velocity to facilitate comparison with the modelling results (Figure 4).
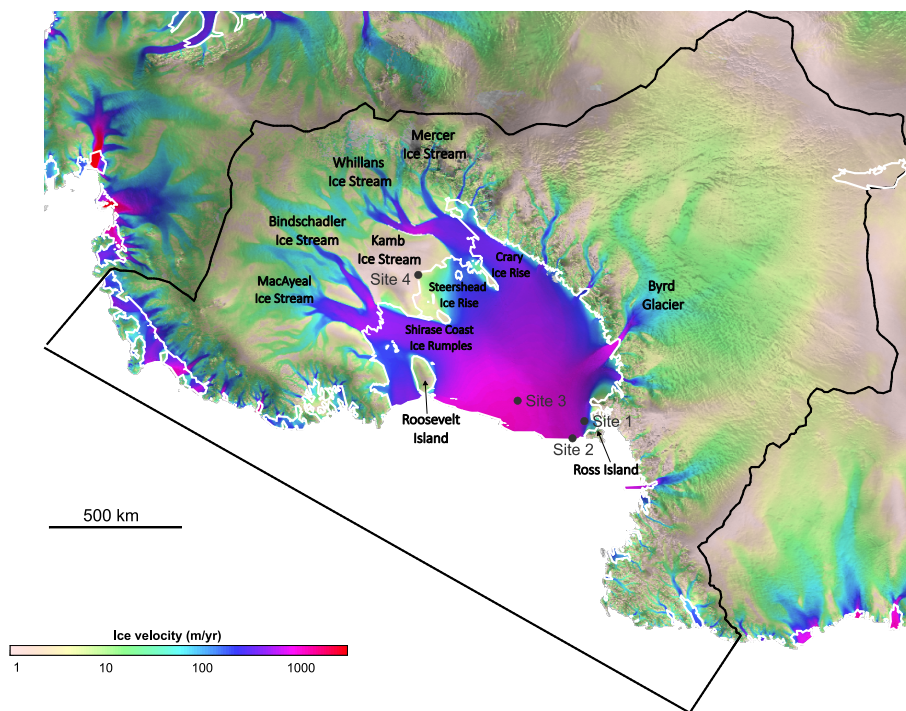
Figure 1. GNSS station locations overlain on modelled Ross Ice Shelf surface velocities. The grounding line is marked in white. GNSS sites shown are: Site 1 (shear margin region), Site 2 (calving front), Site 3 (mid-shelf region), and Site 4 (KIS grounding zone). Other locations discussed in this study are also labelled. These include the Siple Coast Ice Streams: Mercer Ice Stream (MIS), Whillans Ice Stream (WIS), Kamb Ice Stream (KIS), Bindschadler Ice Stream (BIS), and MacAyeal Ice Stream (MacIS). Byrd Glacier (BG) and Ross Island are also labelled. In addition, the ice rises are labelled on the Siple Coast: Crary Ice Rise (CIR), Steershead Ice Rise (SIR), Shirase Coast Ice Rumples (SCIR), and Roosevelt Island. The projection of this map and all others presented is polar stereographic with a true scale at -71° (EPSG:3031).

2.3 Automatic Differentiation

We used Automatic Differentiation (AD, Sagebaum et al., 2019) in the Ice-sheet and Sea-level System Model (ISSM) to explore the influence that changes in basal melt have on the velocity at each GNSS site. The complete model description is available

in Baldacchino et al. (2022). Here, instead of computing the sensitivity of the model's final volume above flotation, we were interested in the sensitivity of the model velocity at these four GNSS sites. AD allowed us to efficiently map by how much the velocity at each site would be affected if we perturbed the ocean-induced melt at the scale of the model mesh.

The model domain covered the entire RIS and has a non-uniform mesh with a resolution of 1 km at the grounding lines and in the shear margins, 20 km in the ice sheet interior, and at most 10 km within the ice shelf. The basal friction coefficient over grounded ice and the ice viscosity parameter of the floating ice, B, was inferred through a data assimilation technique (Morlighem et al., 2010, 2013) to reproduce observed InSAR surface velocities from the MEaSURES data-set (Rignot et al., 2017; Baldacchino et al., 2022). Environmental boundary conditions included RACMO2.3p2 Surface Mass Balance (Van Wessem et al., 2018) and Massachusetts Institute of Technology general circulation (MITgcm) basal melt rates (Losch, 2008; Holland and Jenkins, 1999; Davis and Nicholls, 2019; Baldacchino et al., 2022). The ice sheet model was run forward for 20 years to allow the grounding line position and ice geometry to relax.

After relaxation, we ran the AD model for 6 months and evaluated the sensitivity of the final velocity at each of the four GNSS sites to perturbations in basal melting rates under floating ice, $\dot{M}_b$. Automatic differentiation provided the gradient of the final velocity at each site, v_i, to basal melt: $\mathcal{D}v_i(\dot{M}_b)$. In other words, the first order response of the velocity to a given perturbation $\epsilon\delta\dot{M}_b$ in $\dot{M}_b$ (where $\epsilon \in \mathbb{R}$, and $\delta\dot{M}_b$ was defined over the entire model domain Ω that can be spatially variable) was given by:

$$v_i(\dot{M}_b + \epsilon\delta\dot{M}_b) = v_i(\dot{M}_b) + \epsilon \int_\Omega \mathcal{D}v_i(\dot{M}_b)\,\delta\dot{M}_b\,d\Omega + \mathcal{O}\left(\epsilon^2\right). \tag{1}$$

The gradient, $\mathcal{D}v_i(\dot{M}_b)$ (in m^{-2}), therefore highlighted the regions where the modelled velocity at a given site was most sensitive to changes in $\dot{M}_b$, and the regions where changes in $\dot{M}_b$ would not affect the final velocity at a first order.

This approach provided four sensitivity maps, one for each site. Figure A5 shows the areas where this sensitivity was higher than our threshold value of 2e-11 m^{-2}. The sensitivity threshold value of 2e-11 m^{-2} was chosen to highlight the areas sensitive to basal melt changes. Choosing a lower sensitivity threshold would enlarge the surface area over which the perturbation would need to be applied, and a higher sensitivity threshold would have the opposite effect. We chose a sensitivity value of 2e-11 m^{-2} to highlight areas of high sensitivity over a surface area that is not too restrictive or extensive across the ice shelf (Figure A5). We also included a lower sensitivity value of 0.5e-11 m^{-2} (Figure A6) in our experiments to highlight that the modelled velocity variations are similar for both sensitivity thresholds. These sensitive regions, highlighted in dark red, show where an increase in basal melt rates leads to an increase in ice velocity for each site, and therefore where changes in melt rates would impact ice velocity at these sites the most. Sensitive regions are sometimes hundreds of kilometres from the GNSS stations. Finally, we performed additional experiments where we only perturbed the basal melt rates at the identified sensitive regions along the calving front close to the Ross Island pinning point (Figure A7). These experiments were performed to understand whether seasonal changes in basal melting along the calving front can solely reproduce the seasonal velocity variations observed at the GNSS sites.

2.4 Modelled perturbed basal melt

A set of modelling experiments within ISSM was then performed, where the MITgcm baseline basal melt rates were perturbed seasonally (using a ~~simple~~ sine function) (Figures A8 and A9) at regions identified as highly sensitive in the final AD map ~~(red regions in Figure ??)~~ for each GNSS site:

$$\dot{M}_b(t) = \begin{cases} \text{MITgcm}(t) + p\sin(4\pi + 3t), & \text{if one or more maps shows a sensitivity} > \text{2e-11 m}^{-2} \\ \text{MITgcm}(t), & \text{otherwise} \end{cases} \tag{2}$$

where MITgcm(t) was the unperturbed melt rate from the MITgcm (Figure A8), and p was the amplitude of the perturbation, taken here as 0, 20, 40, 60 or 80 m/a. A sine function with two peaks was used to simulate two basal melt peaks per year (~~these basal melt peaks were either 20, 40, 60 or 80 m/a depending on the perturbation~~ Figure A9). These peaks were modelled in April and October using the + 3 radiant in the sine function. ~~These two~~ Two basal melt peaks per year were needed to ~~replicate~~ reproduce the observed intra-annual velocities at the GNSS sites. The ~~raw~~ unperturbed MITgcm basal melt rates displayed a seasonal signal ~~, however, the~~ with a clear peak in the austral summer, and multiple smaller peaks throughout the year, highlighting that the basal melt rates have large variability (Figure A8). However, the amplitude of this seasonal variability in the baseline MITgcm basal melt rates was not large enough and the phasing incorrect to ~~replicate~~ reproduce the GNSS observed velocity variability. ~~Therefore, we simulated a set of perturbations on top of the raw~~ The MITgcm basal melt rates are imperfect and are unlikely to include all possible temporal and spatial variability in basal melt rates, especially at the grounding lines (Nakayama et al., 2019). Hence the need for perturbations in addition to the unperturbed MITgcm basal melt rates, as described in equation (2) ~~. This~~ (Figure A9). The model was run forward for an additional 20 years to allow the geometry and grounding line to stabilize. The model was then run forward 2 years using the same model setup as described above.

~~Locations where the basal melt rate was perturbed seasonally (i.e., where the AD mapped sensitivity is greater than $2e-11$ m^{-2} (dark red)) for each GNSS site (green markers). The passive ice on the RIS identified by Fürst et al. (2016) is also outlined in black.~~

2.5 Modelled seasonal sea surface height

As discussed previously, Mosbeux et al. (2023) showed that variability in the RIS velocities is driven by seasonal variability in sea surface height (SSH). To explore this potential driver of velocity variability for our new GNSS datasets, we forced our model with the SSH perturbations that Mosbeux et al. (2023) used in their study. Mosbeux et al. (2023) interpolated the SSH forcing from the ocean model of Tinto et al. (2019) as a monthly forcing and applied a parameterisation of the friction in the grounding zone (refer to Mosbeux et al. (2023) for further details). We interpolated the SSH forcing onto our ISSM grid for the RIS, following the same model set-up described in Section 2.3. Mosbeux et al. (2023) highlights that there are two main effects of SSH variability on ice shelf velocities: (1) changes in driving stress and (2) changes in basal stress through grounding line migration. Our modelling experiments are only based on the hydrostatic equilibrium of the grounding line and therefore do not account for the potential role of viscoelasticity (similar to modelling experiment ΔLB2 in Mosbeux et al. (2023)).

3 Results

3.1 GNSS Velocities

3.1.1 Site 1

GNSS velocity observations for Site 1 are presented in Figure 2. Site 1's velocities range from a maximum of 447 m/a to a minimum of 441 m/a with a clear decrease in velocities of 4 m/a over the two years (Figure 2). The velocity variations are small throughout the two years, however, an intra-annual signal is observed at Site 1 (Figure 2). Figure 2 displays two velocity peaks: one in June (austral winter) and one in January (austral summer). These velocity peaks are preceded by periods of acceleration (April - June and November - January) and periods of deceleration (February - April and July - October) (Figure 2). An acceleration of 2 m/a for the ~~velocity~~ peak in June 2020, 1.5 m/a for the ~~velocity~~ peak in January 2021 and 1.5 m/a for the ~~velocity~~ peak in June 2021 highlights the largest seasonal velocity variations at Site 1 (Figure 2).

3.1.2 Site 2

GNSS velocity observations for Site 2 are presented in Figure 2. The velocities range from a maximum of 745 m/a to a minimum of 739 m/a, with a clear intra-annual signal observed at Site 2 (Figure 2). Two distinct velocity peaks are observed at Site 2: one in December (austral summer) and one in July (austral winter). These velocity peaks are preceded by periods of acceleration (April - July and October - December) and periods of deceleration (January - April and July - October) (Figure 2). Similar to Site 1, the velocity variations are small throughout the two years, however, a larger acceleration is observed in the lead-up to the ~~velocity~~ peaks compared to Site 1. An acceleration of 5 m/a for the ~~velocity~~ peak in July 2020, 1.5 m/a for the ~~velocity~~ peak in December 2020, and 3 m/a for the ~~velocity~~ peak in July 2021 highlights the largest seasonal velocity variations at Site 2 (Figure 2). Site 2 displays a larger maximum velocity of 745 m/a compared to Site 1's maximum velocity of 447 m/a. Overall, the velocities neither decreased nor increased significantly throughout the two years at Site ~~2, with the variations in velocities reflecting a clear intra-annual signal.~~ 2.

3.1.3 Site 3

GNSS velocity observations for Site 3 are presented in Figure 2. The velocities range from a maximum of 937 m/a to a minimum of 929 m/a and thus display higher maximum velocities compared to Sites 1 and 2. However, Site 3's intra-annual signal is ~~not similar~~ different to Sites 1 and 2, with a ~~smaller velocity~~ small peak observed in March (austral summer) and a ~~larger velocity~~ large peak in August (austral winter) (Figure 2). These velocity peaks are preceded by periods of acceleration (January - March and April - August) and periods of deceleration (March - April and September - December) (Figure 2). Similar to Sites 1 and 2, the velocity variations throughout the year are small, however, Site 3 displays the largest acceleration in the lead-up to a ~~velocity~~ peak. A small acceleration of 1 m/a for the ~~velocity~~ peak in March 2016 and a much larger acceleration of 8 m/a for the ~~velocity~~ peak in August 2016 is observed (Figure 2). Site 3 was also presented in Klein et al. (2020); Mosbeux et al. (2023) (referred to as DR10), and they display similar results to ours. Both studies display a small velocity peak in January and a large
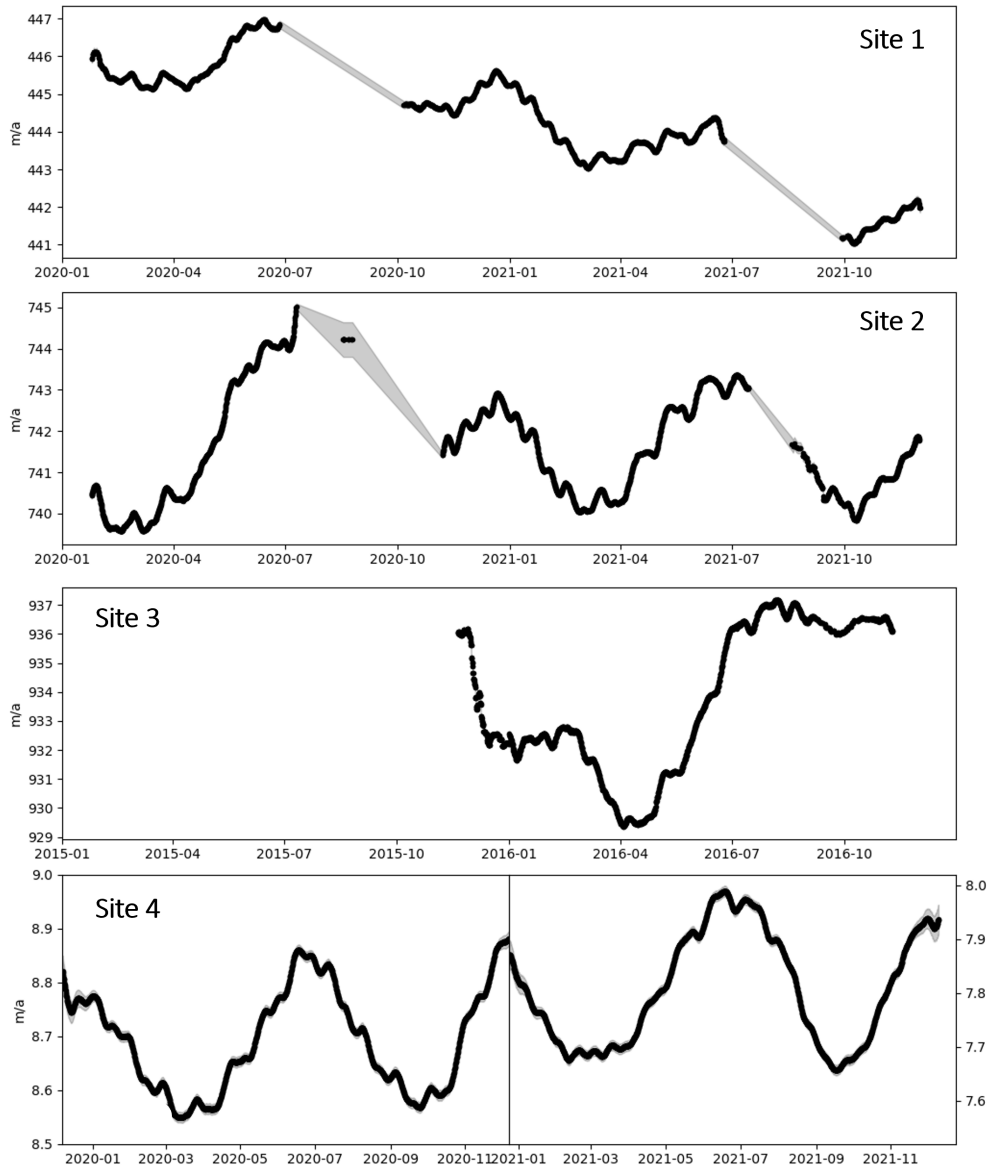
Figure 2. The GNSS velocities (in m/a) at Site 1 (shear margin region~~close to Ross Island~~), Site 2 (~~Coulman High region close to the~~ calving front), Site 3 (mid-shelf region)~~,~~ and Site 4 (~~Kamb Ice Stream~~ KIS grounding ~~line~~zone). The ~~errors~~ uncertainties are provided in the grey windows enclosing the black lines. These ~~errors~~ uncertainties are not visible in a few places, as ~~the errors~~ they are very small. Detrended position and direction for each site is shown in Figures A1-A4

velocity peak in July (Klein et al., 2020; Mosbeux et al., 2023). The velocity variability ranges from -6 m/a in March, and +6 m/a in July, which is a similar range of velocity values found in this study (-7 m/a in April to +1 m/a in August) (Figure 4). However, our velocity peaks for Site 3 (March and August) are offset by 1-2 months compared to the findings presented

 in Klein et al. (2020); Mosbeux et al. (2023). These small differences in the phasing of the intra-annual velocity variability are likely due to small differences in methodology between the studies, such as the use of T-TIDE analysis and the time window used for smoothing the datasets (Klein et al. (2020) used 1-month sliding window, Mosbeux et al. (2023) used longer timescales by using a sliding Gaussian filter with a 2-week standard deviation, and we used a time window of 2 months).

3.1.4 Site 4

GNSS velocity observations for Site 4 are presented in Figure 2. Figure 2 shows that Site 4 has the smallest maximum velocities of 9.0 m/a compared to the other GNSS sites. The KIS has been inactive for the last 160 years and thus the velocities are very low at the grounding line compared to Sites 1, 2, and 3. Site 4 displays a clear intra-annual signal which is similar to Sites 1 and 2 (Figure 2). Two velocity peaks are observed at Site 4 for the years 2020 and 2021: one in December (austral summer) and one in June (austral winter) (Figure 2). Site 4 has the most complete record of GNSS velocity measurements for two years and thus highlights the intra-annual velocity variation nicely. These velocity peaks are preceded by periods of acceleration (March - June and October - December) and periods of deceleration (January - March and July - August) (Figure 2). Site 4 displays the smallest velocity variations compared to the other GNSS sites with an acceleration of 0.4 m/a for the ~~velocity~~ peak in June 2020, 0.3 m/a for the ~~velocity~~ peak in December 2020, 0.3 m/a for the ~~velocity~~ peak in July 2021 and 0.3 m/a for the ~~velocity~~ peak in December 2021 (Figure 2). Klein et al. (2020) also observed that the further the GNSS sites are from the calving front, the smaller the intra-annual velocity variation.

A fortnightly signal is found in the displacement at all GNSS sites and we attribute this to the response of the ice shelf to spring-neap variability in the tidal cycle (Padman et al., 2003; Ray et al., 2021; Rosier and Gudmundsson, 2020). This fortnightly tide-forced variability is dampened by our use of an 8-week window for our velocity estimates (Mosbeux et al., 2023).

3.2 Sensitivity Maps

The AD model produced sensitivity maps show that high sensitivity is observed at the pinning points and ice rises downstream of the Siple Coast ice streams (i.e., Roosevelt Island, Crary Ice Rise, Steershead Ice Rise, and the Shirase Coast Ice Rumples) for all GNSS sites (~~Figure 3~~Figures 1 and 3). For GNSS Sites 1, 2, and 3 we also see high sensitivity to changes in basal melting at the calving front near the Ross Island pinning point. Changes in basal melting can result in detachment from pinning points and ice rises resulting in changes in ice speed (Still et al., 2019; Baldacchino et al., 2022; Reese et al., 2018). Ross Island is a structurally critical region and Gudmundsson et al. (2019) found that rapid melting there influences the flow speed of the entire RIS. Our sensitivity maps confirm this finding, highlighting that changes at and/or near the Ross Island pinning point influence velocities at Sites 1, 2, and 3. It is also important to highlight that Sites 1 and 2 are situated close to the Ross Island pinning point, and thus have high sensitivity to local changes in basal melt.

Additionally, high sensitivity is observed at the Siple Coast Ice Streams and Byrd Glacier grounding lines for Sites 2 and 3 (~~Figure~~ Figures 1 and 3). The grounding lines show high sensitivity because changes in basal melting there can lead to changes in basal friction and grounding line retreat (Baldacchino et al., 2022). These changes in basal friction can drive changes in the
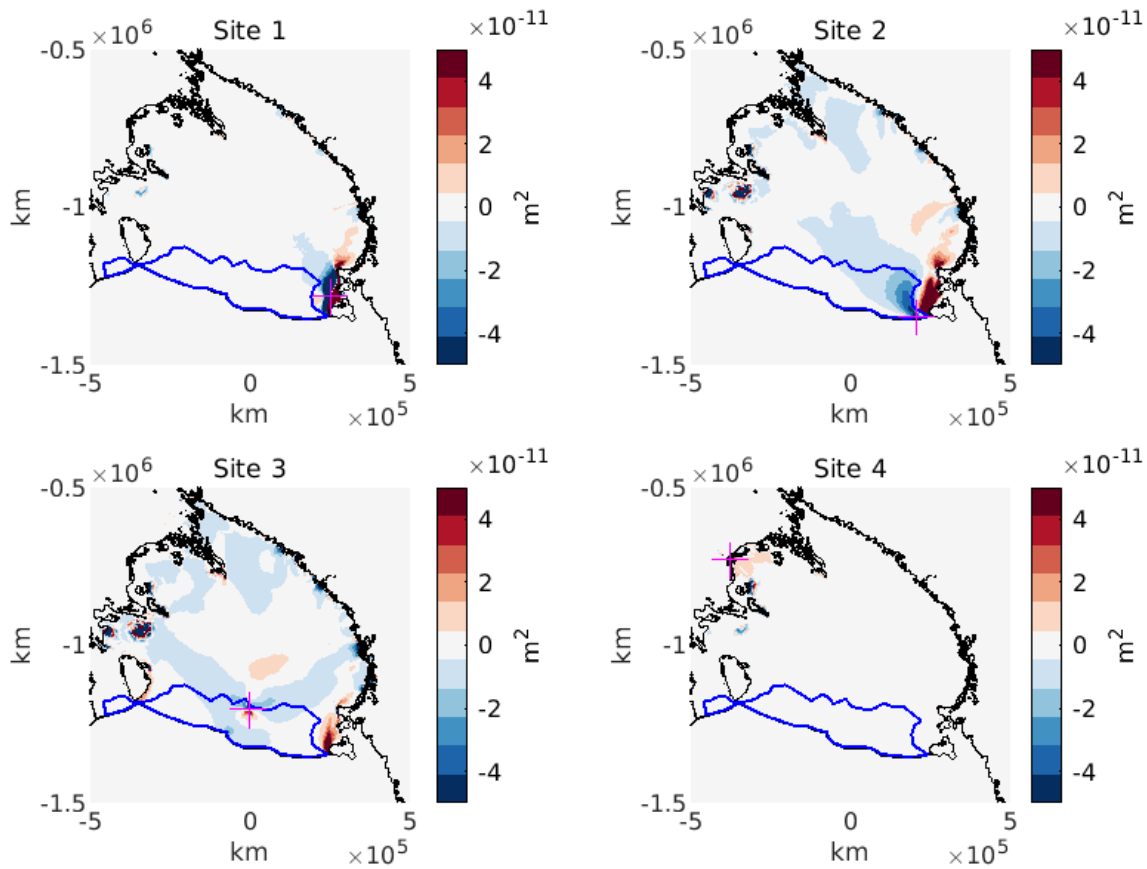
Figure 3. Sensitivity maps of the final velocity at each of the four GNSS sites to basal ~~melting~~ melt rates under floating ice $\dot{M}_b$ over 40 years (in m^{-2}). The sensitivity maps highlight that an increase or decrease in basal melt rates at identified sensitive regions increases or decreases the velocities at the GNSS sites. The grounding line (black line) and passive ice (blue line) on the RIS identified by Fürst et al. (2016) ~~is outlined in black~~are highlighted. The GNSS sites are identified using ~~green~~ pink markers.

ice streams and outlet glaciers' flow dynamics and discharge (Baldacchino et al., 2022; Pattyn, 2017; Shepherd et al., 2018). We observe high sensitivity at the near-stagnant KIS grounding zone for Site 4, and no sensitivity elsewhere for this GNSS site. This high sensitivity at the KIS grounding zone highlights that local changes in basal melt at the grounding zone can influence the velocities at Site 4 and changes in basal melt elsewhere on the ice shelf do not affect Site 4 velocities.

Finally, high sensitivity within the interior of the ice shelf and directly downstream of active ice streams and outlet glaciers is observed for GNSS Sites 2 and 3 (~~Figure~~ Figures 1 and 3). Sensitivity to changes in basal melting is also observed at the "passive" region (~~black~~ blue outline in Figure 3 identified by Fürst et al. (2016)) for GNSS Sites 2 and 3. This indicates that

360

local changes in basal melt affect the velocities at Sites 2 and 3 as both these sites are located in the "passive" region. Overall, the sensitivity maps show that GNSS Sites 2 and 3 velocities have high sensitivity to basal melting across the majority of the ice shelf, compared to Sites 1 and 4, which have higher sensitivities to local changes in basal melting.

3.3 Modelled Velocities

The modelled velocity variations are compared to the GNSS velocity variations (change from the initial velocity) for each site in Figure 4. We model two distinct velocity peaks: one in January (austral summer) and one in June (austral winter) for the basal melt perturbation experiments. We perturbed the basal melt rates seasonally at the identified sensitive regions to ~~replicate~~ reproduce these two velocity peaks at all the GNSS sites. These sensitive regions are located at the calving front near the Ross Island shear zone for Sites 1, 2, and 3 and pinning points downstream of the Siple Coast Ice Streams and at their grounding lines for Sites 2, 3, and 4. For all GNSS sites, we observe that the intra-annual velocity variation is small when we perturb the basal melt rates by a magnitude of 20 m/a, and this intra-annual velocity variation quadruples when we perturb the basal melt rates by a magnitude of 80 m/a (Figure 4). The dotted black line in Figure 4 highlights the ~~model~~ experiments which used the lower sensitivity value of 0.5e-11 m^{-2} (Figure ~~A1~~A6). Figure 4 shows that for ~~all GNSS sites~~ GNSS Sites 1, 2, and 3 the use of the lower sensitivity value did not significantly affect the final modelled velocity variations. However, for Site 4 the use of a lower sensitivity threshold increased the velocity peaks by about 20% due to more sensitive areas near the KIS grounding zone being perturbed. Additionally, the solid black line in Figure 4 highlights the experiments in which the basal melt was only perturbed at the calving front near Ross Island. Figure 4 shows that for Sites 1, 2, and 3 the perturbation of basal melt rates close to Ross Island produces similar velocity variations to the other model experiments. However, for Site 4 the velocity variations are much smaller due to being insensitive to the perturbed regions. The modelled absolute velocity values are similar to the GNSS absolute velocity values for Site 1 but are larger than the GNSS absolute velocity values for Sites 2, 3~~and 4.~~, and 4 (Figure A10). However, in this ~~paper~~study, we focus on ~~replicating~~ reproducing and analysing the GNSS velocity variations in our model simulations~~and thus, focus on these results~~.

Our basal melt perturbed model predicts an intra-annual variation in velocity at Site 1 ranging from 1 m/a to 5 m/a for 20 m/a basal melt perturbation ~~, 4 m/a to 12 m/a for 40 m/a basal melt perturbation, 5 m/a to 18 m/a for 60 m/a basal melt perturbation~~ and 6 m/a to 28 m/a for the 80 m/a basal melt perturbation (Figure 4). An acceleration of 4 m/a for the velocity peaks in January and June is observed in the 20 m/a basal melt perturbed model experiments, which is most similar to Site 1's GNSS observed accelerations of 2 m/a for the velocity peak in June 2020, 1.5 m/a for the velocity peak in January 2020 and 1.5 m/a for the velocity peak in June 2021 (Figure 4). The seasonal SSH perturbed model displays no intra-annual velocity variability for Site 1 (Figure 4). However, the SSH forced velocities decrease over time similar to the GNSS observations (Figure 4).

The basal melt perturbed modelled intra-annual velocity variations at Site 2 range from 0 m/a to 3 m/a for 20 m/a basal melt perturbation ~~, 2 m/a to 6 m/a for 40 m/a basal melt perturbation, 2 m/a to 9 m/a for 60 m/a basal melt perturbation~~ and 2 m/a to 13 m/a for the 80 m/a basal melt perturbation (Figure 4). The phasing of the modelled velocity peaks (January and June) are offset by one month compared to the GNSS observed velocity peaks (December and July) at Site 2 (Figure 4). However, the peak in velocity occurs at the end of December, and the beginning of July which is similar to our modelled velocity peaks in
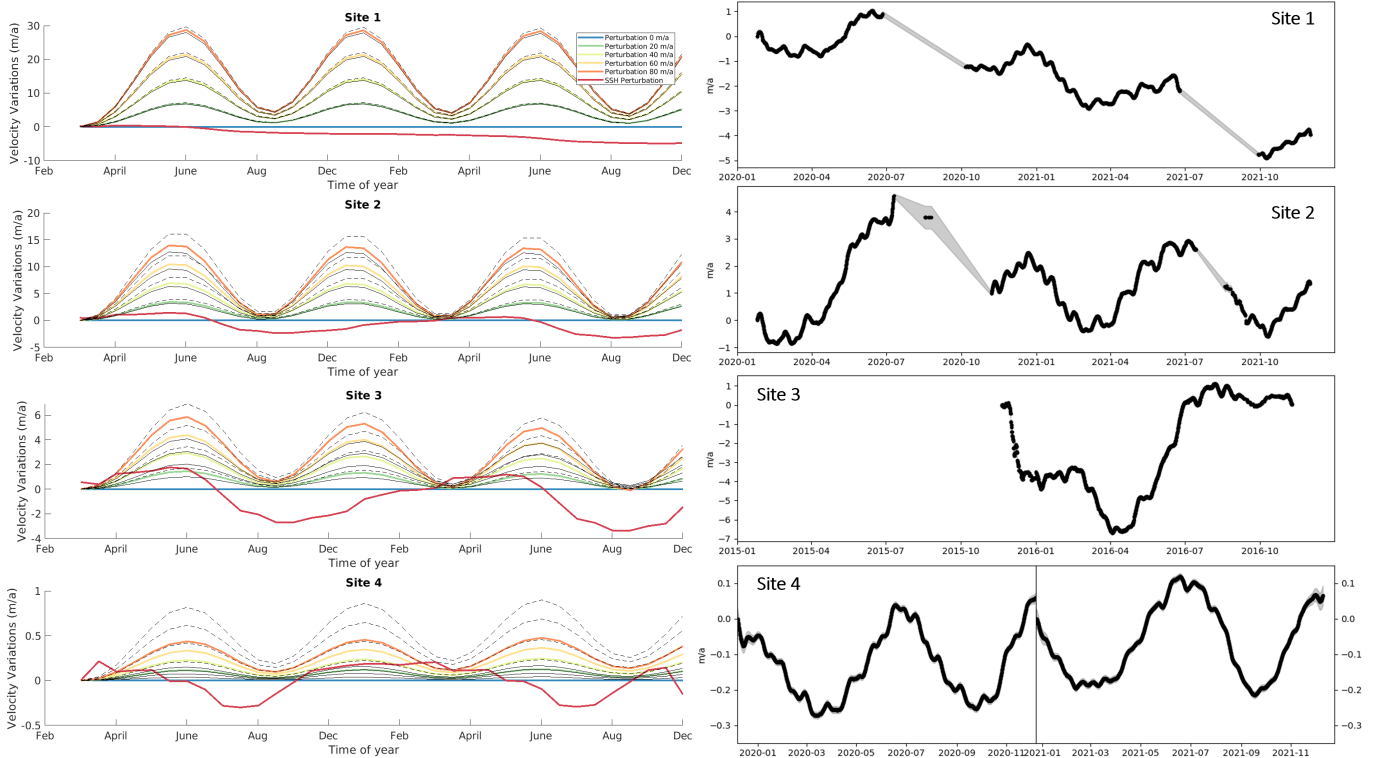
Figure 4. The ~~GNSS~~ modelled (~~right~~left) and ~~modelled~~ GNSS (~~left~~right) velocity variations (in m/a) at each GNSS site: Site 1 (shear margin region), Site 2 (~~Coulman High region~~calving front), Site 3 (mid-shelf region), and Site 4 (KIS grounding zone). The dotted black line represents the additional sensitivity threshold value experiment and the solid black line represents the additional sensitivity experiment where we only perturbed the basal melt rates at the calving front close to Ross Island.

January and June. The 20 m/a basal melt perturbed modelled velocity variation is similar in amplitude to the GNSS velocity

400 variations. An acceleration of 3 m/a for the ~~velocity~~ peaks in January and June is observed in the 20 m/a basal melt perturbed model experiments, which is most similar to Site 2's GNSS observed accelerations of 5 m/a for the ~~velocity~~ peak in July 2020, 1.5 m/a for the ~~velocity~~ peak in December 2020 and 3 m/a for the ~~velocity~~ peak in July 2021 (Figure 4). The seasonal SSH perturbed model displays an intra-annual velocity variability with a different phasing and amplitude to the GNSS observations at Site 2 (Figure 4). The SSH forced velocities display one distinct peak per year (late May), with a velocity minimum displayed

405 in August (Figure 4).

For Site 3, the modelled intra-annual velocity variations range from 0 m/a to 1 m/a for 20 m/a basal melt perturbation ~~, 0.5 m/a to 2 m/a for 40 m/a basal melt perturbation, 1 m/a to 2.5 m/a for 60 m/a basal melt perturbation~~ and 1.5 m/a to 4 m/a for the 80 m/a basal melt perturbation (Figure 4). The modelled velocity peaks occur in January and June, which is different from the GNSS observed velocity peaks in March and August for Site 3 (Figure 4). Therefore, the phasing of the modelled

410 velocity variations is offset by a couple of months. Additionally, the amplitude of the modelled velocity peaks is smaller

compared to the GNSS observed velocity peaks at Site 3. An acceleration of 1 m/a for the ~~velocity~~ peak in March ~~2016~~ and 8 m/a for the ~~velocity~~ peak in August ~~2016~~ is observed by the GNSS receiver at Site 3 (Figure 4). None of the basal melt perturbed modelled velocity variations capture an acceleration of 8 m/a in August (Figure 4). Overall, the amplitude of the modelled velocity variation is significantly smaller compared to the GNSS measurements at Site 3. We display two velocity peaks, whereas Klein et al. (2020) displayed one velocity peak in late May, with a smaller velocity range (-0.18 to +0.18 m/a). This is likely due to the type of perturbations (i.e., magnitude and phasing) used in this study. Furthermore, the seasonal SSH perturbed model displays an intra-annual velocity variability with a different phasing to the GNSS observations (Figure 4). The SSH forced velocities display one peak per year, similar to Site 2, in late May, with a velocity minimum displayed in August. However, Site 3 displays one distinct peak per year similar to the SSH forced velocity variability, and there is a closer similarity in the amplitude of velocity variations between the SSH forced velocities and the GNSS observations (Figure 4). Mosbeux et al. (2023) modelled a velocity peak in August for Site 3, highlighting that our modelled velocity peak is offset by a couple of months. This may be due to our modelling experiments not taking into account the potential role of viscoelasticity.

Finally, we model the ~~smallest~~ lowest intra-annual velocity variation at Site 4 when perturbing the basal melt rates, which is similar to the GNSS measurements (Figure 4). The modelled intra-annual velocity variations at Site 4 range from 0.01 m/a to 0.04 m/a for 20 m/a basal melt perturbation ~~, 0.02 m/a to 0.06 m/a for 40 m/a basal melt perturbation, 0.03 m/a to 0.1 m/a for 60 m/a basal melt perturbation~~ and 0.04 m/a to 0.15 m/a for the 80 m/a basal melt perturbation (Figure 4). The phasing of the modelled velocity variations is similar to the GNSS-measured velocity variations with a clear intra-annual signal observed at Site 4. The modelled velocity peaks occur in January and June which is similar to the GNSS-measured velocity peaks at the end of December and in June (Figure 4). However, none of the ~~basal melt perturbed~~ modelled velocity variations ~~could replicate~~ of the basal melt perturbation experiments could reproduce the amplitudes of the GNSS observed velocity variations. An acceleration of 0.4 m/a for the ~~velocity~~ peak in June 2020, 0.3 m/a for the ~~velocity~~ peak in December 2020, 0.3 m/a for the ~~velocity~~ peak in July 2021 and 0.3 m/a for the ~~velocity~~ peak in December 2021 (Figure 4). An acceleration of 0.11 m/a for the ~~velocity~~ peaks in January and June is observed in the 80 m/a basal melt perturbed model experiments and is most similar to the GNSS-measured velocity variations at Site 4. Similarly, to Site 3, overall the amplitude of the modelled velocity variation is significantly smaller compared to the GNSS measurements at Site 4. The seasonal SSH perturbed model displays an intra-annual velocity variability with one velocity peak per year (February) (Figure 4). This phasing is different from our GNSS observations which display two distinct velocity peaks per year (December and June). However, the amplitude of velocity variations is most similar to the GNSS observations, ranging from -0.4 to 0.3 m/a (Figure 4).

For all GNSS sites, an increase in basal melt rates accelerates the velocities compared to the control run (Figure 4). We would expect this as the seasonally elevated melt rates lead to short-term thinning and acceleration of the ice shelf (Gudmundsson et al., 2019; Campbell et al., 2018). The amplitude of modelled velocity variability decreases with increasing distance from the calving front, with the largest velocity variations modelled at Sites 1 and 2, and the smallest at Site 4. However, the GNSS units record the largest amplitude in velocity variation at Site 3 which also agrees with Klein et al. (2020) and Mosbeux et al. (2023).

4 Discussion

4.1 Intra-annual velocity variability

~~There is a clear seasonal signal for all GNSS sites with two velocity peaks: one in austral summer and one in austral winter (Figures 2 and 4). We observe that the magnitude of variation in velocities is larger for Sites 1, 2, and 3 compared to Site 4, likely due to the proximity of these sites to the calving front and seasonally elevated basal melt rates (Klein et al., 2020; Mosbeux et al., 2023). We model a similar intra-annual velocity variability (in both~~ The model captures a seasonal signal in velocity that is similar in phasing and magnitude ~~) at GNSS~~ to the GNSS observations at Sites 1 and 2 ~~using seasonally perturbed basal melt magnitudes~~ when perturbing basal melt rates (with a magnitude of 20 m/a~~at the identified sensitive regions(Figures ??, 3 and 4)~~) at sensitive regions. However, for Site 3, the magnitude of the modelled velocity variability is significantly smaller and the phasing of the modelled velocity variability is offset by a couple of months compared to the GNSS measurements for all basal melt perturbations (Figure 4). Additionally, for Site 4 the modelled velocity variability has a similar phasing to the GNSS measurements, but an 80 m/a basal melt perturbation is needed ~~at this site~~ to model a similar ~~magnitude~~ amplitude in velocity variability. This may indicate that ~~larger basal melt rates are needed at sensitive regions to replicate the intra-annual velocity variations at Sites 3 and 4 or~~ a combination of mechanisms may be driving these velocity variations ~~. The ice sheet model used in this paper does not account for varying forcings other than the seasonal cycle of basal melting~~at Sites 3 and 4. We also show that seasonal variability in SSH alone cannot reproduce the two velocity peaks observed at the new GNSS sites (Sites 1, 2 and 4).

In the modelling experiments, basal melt rates that peak in October and April are required to ~~replicate~~ reproduce the observed velocity peaks in austral summer (December and/or January) and austral winter (June and/or July) at Sites 1, 2 and 4 (Figures 2 and 4). Our modelled basal melt perturbations highlight that there is a delay of ~~2 - 3~~ 2-3 months between the peak basal melt rates and ~~peak~~ velocities. We suggest this delay is due to the time it takes for the basal melt rates to thin the ice shelf significantly enough to change the stress regime at the GNSS sites. Previous studies have found that lag times in the ice shelf flow response occur due to the time required for basal melting to cause sufficient thinning (thickening) to produce an observable acceleration (deceleration) of the ice shelf (Christianson et al., 2016; Greene et al., 2017; Roberts et al., 2018). Roberts et al. (2018) suggest that the time delay between basal melting and velocity change depends on the proximity of the region of interest to the highest basal melt rates and the thickness of that region (i.e., thicker areas have a greater lag time) (Greene et al., 2018). In this ~~paper~~study, we are perturbing basal melt rates at identified sensitive regions of the ice shelf that exist both locally and up to ~~1000km~~ 1000 km away from the GNSS sites (Figure ~~??~~A5). We hypothesize that the velocities reach a maximum in austral summer (December and/or January) and austral winter (July and/or June) as the ice within these sensitive regions has thinned significantly during periods of peak melting in October and April (Figures 2 and 4). Greene et al. (2018) also found that the Totten Ice Shelf velocity maxima occurs at the end of the high melt season in July when the ice thickness reaches a minimum.

Sensitive regions identified from the AD experiments are located often at or near pinning points (~~Figure ??~~Figures A5, A6 and A7). Such areas are important for ice shelf stability and buttressing (Pattyn, 2017; Still et al., 2019; Matsuoka et al., 2015; Gudmundsson et al., 2019; Lhermitte et al., 2020). Figure ~~?? highlights that basal melt rates are perturbed~~ 3 shows that velocities at Sites 1, 2, and 3 are most sensitive to basal melt rate perturbations at the Ross Island region~~for Sites 1, 2 and 3.~~.

Ross Island is an important pinning point for the RIS, with changes in ice thickness here found to significantly impact overall ice shelf dynamics (Reese et al., 2018; Gudmundsson et al., 2019). On floating ice shelves, basal drag is negligible and the lateral drag depends on the existence of ice shelf margins and/or pinning points (Dupond and Alley, 2005; Gudmundsson et al., 2019; Gudmundsson, 2013). Ice shelf thinning can reduce the thickness of shear margins and the contact area over pinning points and ice rises, which decreases the lateral drag and the buttressing ability of the ice shelf (Shepherd et al., 2004; Joughin et al., 2021; Gagliardini et al., 2010; Feldmann et al., 2022). This reduction in buttressing has a near-instantaneous effect on ice shelf acceleration (Larter, 2022; Arndt et al., 2018; Joughin et al., 2021; Dupond and Alley, 2005; Gudmundsson et al., 2019). Roberts et al. (2018) also observed that ice shelf thinning (thickening) was coincident with faster (slower) velocities due to changes in resistive stresses at ice rumples present on the Totten Ice Shelf. ~~Therefore, thinning at and/or near pinning points and ice rises will reduce the resistive stresses on the ice shelf and impact the velocities at the GNSS sites. The observed lag is likely due to the time it takes for the basal melt rates to thin the ice shelf enough at the identified sensitive regions to reduce the resistive stresses.~~

Additionally, we perturb basal melt rates at the KIS grounding zone to try and ~~replicate~~ reproduce the intra-annual ~~signal observed~~ velocity signal at Site 4. Changes in basal melting ~~at grounding zones will dictate the temperature gradient of the ice and the rate of basal melting, affecting basal friction and ice rigidity around the grounding line~~ near the grounding zones generally lead to ice thinning and grounding line retreat (Baldacchino et al., 2022; Ranganathan et al., 2021). This can cause changes in basal stresses, ~~grounding line position,~~ ice velocities, and discharge of the ice stream and/or outlet glacier ~~(Baldacchino et al., 2022; Horgan et al., 2021; Anandakrishnan et al., 2007). We suggest that changes in basal melting at the KIS grounding zone could modify the driving stresses and velocities at Site 4 by altering the basal friction. Additionally, changes in basal friction reduce the resistive stresses at~~ (Baldacchino et al., 2022; Anandakrishnan et al., 2007). Additionally, ice thinning reduces the buttressing effect from ice rises downstream of the KIS grounding zone, which drive changes in the velocities at Site 4 and elsewhere on the ice shelf.

4.2 ~~Basal~~ Comparison to observed basal melt rates ~~on~~ beneath the Ross Ice Shelf

~~We can replicate similar intra-annual velocity variations to the GNSS measurements at Sites 1 and 2 by seasonally perturbing~~ The basal melt rates used in this study are high for the Ross Ice Shelf today, however, our focus here is on asking whether perturbations in basal melt rates can reproduce a similar velocity variability as observed by the GNSS units. We found that seasonal perturbations in basal melt rates (with a magnitude of 20 m/a~~.~~) can reproduce a similar velocity variability for Sites 1 and 2. Our AD-inferred sensitivity map shows that we do not need 20 m/a of perturbation under the entire ice shelf, but only over 2% of the ice shelf (i.e., identified sensitive regions)~~to reproduce the intra-annual velocity variations at Sites 1 and 2. However, is this basal melt perturbation realistic at the identified sensitive regions on the RIS?~~. In this section, we suggest that the ~~basal melt perturbations we have~~ melt rate perturbations used in our modelling experiments are ~~realistic~~ more probable for Sites 1 and 2 ~~but less realistic~~ than for Sites 3 and 4.

Firstly, we perturbed the basal melt rates to peak in April and October to reproduce the observed intra-annual velocity variability on the ice shelf (Figures 2 and 4). Stewart et al. (2019) ~~shows that the timing of these basal melt peaks is realistic~~

~~for the RIS~~ displays large variability in basal melt rates throughout the year near the calving front of the RIS. Stewart et al. (2019) observes a large basal melt peak in the austral summer (January - March) > 3 m/a and smaller basal melt peaks in early winter (April and/or May) and late winter (October and/or November) of ~~1 - 2~~ 1-2 m/a at the calving front near the Ross Island pinning point. Additionally, Stewart et al. (2019) observe that the basal melt rates during winter are "~~still~~ an order of magnitude higher than the ~~satellite-inferred shelf-wide average and contribute substantially to the high average melt rates. " He suggests~~ satellite measured ice shelf average. They suggest that these higher basal melt rates during the early winter are due to the remnant heat from the summer AASW inflow and in late winter are due to the inflows of HSSW into the ice shelf cavity when large heat loss and sea ice production leads to active cross-frontal flow that ventilates the cavity (Stewart et al., 2019; Jendersie et al., 2018; Årthun et al., 2013). Figure A8 also shows the large variability in the baseline MITgcm basal melt rates similar to the observations made by Stewart et al. (2019), highlighting that basal melt rates have more variability than presented in Klein et al. (2020). Additionally, Klein et al. (2020) suggests that the actual total summer increase in the heat content of the AASW layer near the ice front is likely to be larger than their modelled increase, and the seasonal enhancement of the basal melting will continue further into autumn than in their model. Klein et al. (2020) extended the late melt period to April and found that this also shifted the timing of maximum velocity a month later, suggesting that a longer or later melt period at the front could have aligned their modelled and observed velocity phases similar to our results in this study. These findings support the timing of our perturbed basal melt rate peaks in April and October ~~for the identified sensitive regions~~ at the calving front near ~~the Ross Island shear zone~~ Ross Island which influences the velocities at Sites 1, 2, and 3.

Secondly, we perturb the basal melt rates with a range of magnitudes (20-80 m/a) to try and reproduce the observed velocity variability at the GNSS sites. We perturb the basal melt rates near the Ross Island shear zone by a magnitude of 20 m/a for Sites 1 and 2 to reproduce ~~similar~~ intra-annual velocity variations similar to the GNSS measurements (Figures ~~??~~3, 2 and 4). The RIS has low annual average basal melt rates across the ice shelf (~~0 - 1~~ 0-1 m/a), with the highest average basal melt rates observed at the ice shelf front (> 3 m/a), near ~~the~~ Ross Island pinning point (Stewart et al., 2019; Stevens et al., 2020; Das et al., 2020; Adusumilli et al., 2020; Schodlok et al., 2016; Assmann et al., 2003; Holland et al., 2003; Stern et al., 2013). Figure 5 shows that MITgcm maximum ~~short-term~~ summer basal melt rates along the calving front are ~~10 - 25~~ 10-25 m/a, which is similar to our basal melt perturbation of 20 m/a for Sites 1 and 2. Stewart et al. (2019) also observed ~~short-term~~ summer basal melt rates of ~~10 - 50~~ 10-50 m/a at the calving front near ~~the Coulman High region and Ross Islandshear zone~~Ross Island. However, ~~these~~ the modelled (Figure 5) and observed (Stewart et al., 2019) basal melt magnitudes of 20 m/a occur during the austral summer, and we perturb basal melt rates in early and late austral winter.

~~Summer elevated basal melt rates at the calving front are expected to increase due to continued surface warming and changes in sea ice cover (Das et al., 2020; Stevens et al., 2020; Stern et al., 2013; Stewart et al., 2019; Horgan et al., 2011; Porter et al., 2019; Tinto . The basal melt rates have not been observed to increase by the same magnitude as we have perturbed in the model experiments (20 m/a) in early and late winter, but this may be possible in the future if basal melt rates continue to increase (Stewart et al., 2019; Porter et a and/or changes in primary modes of basal melting occur (Tinto et al., 2019). Clem et al. (2018) suggests that the switching of the Interdecadal Pacific Oscillation to its positive phase in the coming decade could increase intrusions of CDW onto the continental shelf. These increased intrusions of the CDW onto the continental shelf will form mCDW which would reduce~~

~~sea ice formation in the Ross Sea and enhance basal melting of the RIS (Tinto et al., 2019; Reddy et al., 2007). Additionally, Greene et al. (2022) suggest that the RIS will experience calving by the end of the century which may reshape the ocean~~
550 ~~environment at the ice shelf front and elevate basal melt rates under the ice shelf.~~

~~For~~ However, for Site 3, none of the basal melt perturbations were able to ~~replicate similar~~ reproduce intra-annual velocity variations similar to the GNSS measurements. This suggests that ~~larger basal melt~~ if melt is responsible then larger perturbations may be needed at the identified sensitive regions to ~~replicate~~ reproduce the observed velocity variability~~at Site 3.~~. However, basal melt magnitudes of > 80 m/a are highly unrealistic for the RIS today (Adusumilli et al., 2020)~~and in the~~
555 ~~future~~. Therefore, we suggest that Site 3's current observed intra-annual velocity variations may be driven by a combination of mechanisms not captured by our model.
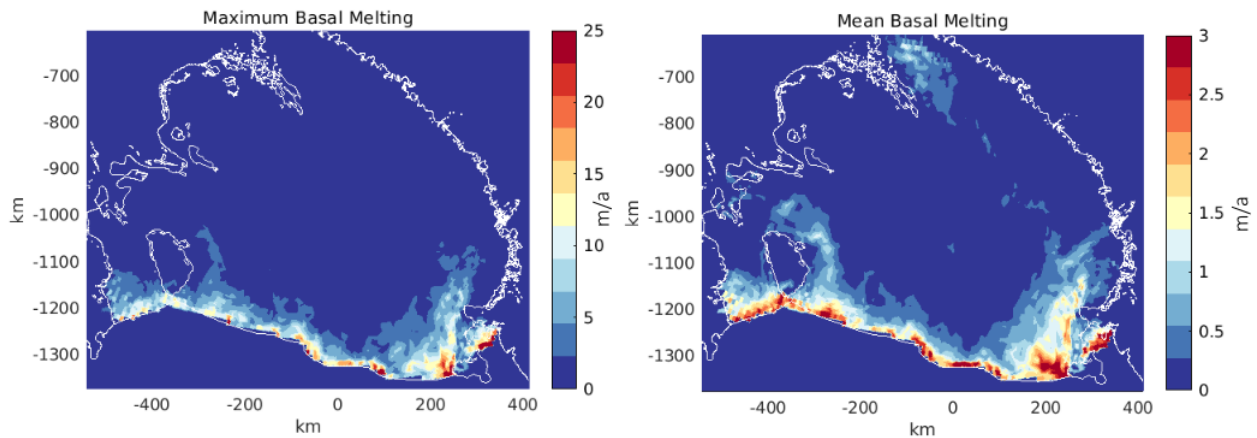
Figure 5. MITgcm ~~short-term~~ summer maximum and mean basal melt rates (in m/a) on the RIS.

Additionally, for Site 4 we perturb basal melt rates with magnitudes of 80 m/a at the KIS grounding zone and Siple Coast ice rises to ~~simulate the~~ reproduce intra-annual velocity variability. Perturbed basal melt magnitudes of 80 m/a are unrealistically high for the interior of the ice shelf, with observed basal melt rates being low (~~0 - 1~~ 0-1 m/a (Adusumilli et al., 2020)). Localised
560 high basal melt rates of 22.2±0.2m/a have been observed near grounding lines of the Siple Coast Ice Streams (Marsh et al., 2016). However, no basal melt rates of 80 m/a have been observed on seasonal timescales at the Siple Coast grounding lines or pinning points and ice rises. Seasonally pronounced basal melt predominantly occurs along the RIS front (Jacobs et al., 1992), with Stewart et al. (2019) and Horgan et al. (2011) observing that the seasonal basal melt rates decrease with distance from the calving front. The interior of the ice shelf has a residence time of ~~1 - 6~~ 1-6 years for sub-ice-shelf waters resulting in basal melt
565 rates varying on much longer timescales (Stevens et al., 2020; Reddy et al., 2010; Michel et al., 1979; Smethie Jr and Jacobs, 2005). Therefore, it is unlikely that Site 4's observed intra-annual velocities are driven by seasonal changes in basal melt rates.

We also perturb basal melt rates at the Siple Coast pinning points and ice rises to ~~simulate~~ reproduce intra-annual velocity variations at Site 2. It is unlikely that seasonally varying basal melt rates at the Siple Coast pinning points and ice rises

are driving the velocity variations at Site 2. We suggest that the seasonal basal melt variability observed at the calving front is driving the majority of Site 2's intra-annual velocity variability . We performed additional experiments where we only perturbed the basal melt rates at the identified sensitive regions along the calving front close to the Ross Island pinning point. These experiments showed that the phasing and magnitude of velocity variations for Sites 1 and 2 were similar to the experiments presented in this paper, supporting our suggestion that the majority of Site 2's intra-annual velocity variability is driven by seasonal changes in basal melting at the calving front. (Figure 4).

4.3 Other potential drivers of intra-annual velocity variability

We suggest highlight that seasonal changes in basal melt can explain reproduce the observed intra-annual velocity variations at Sites 1 and 2, using perturbed basal melt rates with magnitudes of 20 m/a at the calving front. We also suggest Our study differs from Klein et al. (2020) due to: (1) our new GNSS datasets for Sites 1 and 2 displaying two velocity peaks per year, whereas Site 3 only displayed one velocity peak per year, (2) we use weekly MITgcm basal melt rates which can capture intra-annual variability in atmospheric, oceanic and sea-ice conditions in the Ross Sea and (3) we use the AD model to identify sensitive areas of the ice shelf, and then perturb basal melt rates at these sensitive areas. However, we also highlight that seasonal changes in basal melt cannot explain reproduce the observed intra-annual velocity variations at Sites 3 and 4. We were unable to model similar intra-annual velocity variations to the GNSS measurements for Site 3 using the basal melt perturbations consistent with the findings of Klein et al. (2020). Additionally, for Site 4, we were able to model similar reproduce the observed intra-annual velocity variations using an unrealistically extremely high perturbed basal melt rate of 80 m/a at the KIS grounding zone and ice rises downstream of the Siple Coast ice streams, where no evidence of seasonally high basal melting rates has been observed. In Therefore, in this section, we discuss other potential drivers of the observed intra-annual velocity variability at Sites 3 and 4.

Most recently, Mosbeux et al. (2023) has shown that the seasonal variability of Sea Surface Height sea surface height (SSH) modifies ice velocity by changing (1) the driving stress by locally tilting the ice shelf and (2) the basal condition in the grounding zone. They suggested that SSH variations can lead to changes in bed stresses at the grounding zone, with a negative SSH at the grounding line causing a slow down of ice flow through an increase in basal drag (Mosbeux et al., 2023). Therefore, the intra-annual velocity variations observed at Sites 3 and 4 in this paper could potentially be explained by the seasonal cycle of However, we show that seasonal variability in SSH alone cannot reproduce the two velocity peaks per year observed at our new GNSS sites. We suggest that Mosbeux et al. (2023) was able to reproduce the velocity variability recorded at Site 3 due to implementing additional parameterization of viscoelastic processes in their model. However, Mosbeux et al. (2023) did not observe a seasonal velocity variation close to the grounding line of the Whillans Ice Stream when forced by SSH variations, and thus this needs further exploration for the KIS grounding zone seasonal variations in SSH are likely providing a small additional contribution to velocity changes on the RIS as indicated by Mosbeux et al. (2023) and shown by the similarity in velocity amplitudes at Sites 3 and 4 to the GNSS measurements.

Additionally, Greene et al. (2018) found that changes in buttressing from sea ice can explain the seasonal cycle of Totten Glacier's ice shelf velocities. Sea ice cover in the Ross Sea decreases in the summer months and increases in the winter months,

suggesting that ice shelf velocities would increase in the austral spring and decrease in the austral winter if forced by variations in sea ice backstress (Greene et al., 2018; Cassotto et al., 2015; Howat et al., 2010). However, we observe an acceleration in ice shelf velocities in austral summer and austral winter, indicating that the GNSS velocity variations are not forced by variations in sea ice backstress.

Seasonal variations in surface air temperatures can also influence the surface melt rates of the ice shelf (Nicolas et al., 2017a; Trusel et al., 2015; Zou et al., 2021a, b) and drive variations in velocities. For example, it has been shown that surface meltwater influences ice shelf velocity by percolating through and weakening the ice shelf shear margins ~~(Cavanagh et al., 2017; Liu and Miller, 1979;~~ (Cavanagh et al., 2017; Liu and Miller, 1979; Vaughan and Doake, 1996; Greene et al., 2018; Alley et al., 2018). However, the surface melt rates on the RIS are small, and the response of the ice shelf velocities to summer elevated surface melting has been shown to occur over short timescales (hours to weeks) (Stevens et al., 2022; Chaput et al., 2018; Nicolas et al., 2017a). An El-Niño event occurred in the summer of 2015/2016 when the GNSS measurements for Site 3 were recorded. This event may have increased surface melt rates on the RIS as well as modified wind patterns and ocean circulation (Klein et al., 2020; Paolo et al., 2015). Nicolas et al. (2017b) observed 14 days of enhanced surface melting on the RIS, between the 10th and 21st of January 2016 due to persistent air temperatures higher than -2°C in the region of Site 3 (Klein et al., 2020; Chaput et al., 2018). ~~These high surface melt rates may have influenced the observed peak in velocities at Site 3 in March 2016 (Figure 2).~~ Klein et al. (2020) suggests that the surface heat fluxes over the ocean during this surface melt event may have been substantially different than those used to drive the ocean models. Therefore, the MITgcm basal melt rates likely do not take into account this high surface melt event and this may explain why we cannot reproduce the intra-annual velocity variability observed at Site 3.

~~Some Siple Coast ice stream velocities are modulated by tidal forcing of the floating ice shelves (Bindschadler et al., 2003; Anandakrishn~~ ~~.~~ Tides are known to cause substantial variations in velocity over short periods (Anandakrishnan et al., 2003; Gudmundsson, 2006; Bindscha and longer periods of up to a year (Murray et al., 2007). However, Klein et al. (2020) highlighted that the vertical signals of tides are too small to provide a significant forcing to the horizontal movement of the RIS through non-linear ice-ocean processes along the grounding zone as suggested by Murray et al. (2007). Our GNSS processing smooths out short-term tidal effects, but daily variability is likely to be large, with the Ross Sea tides being almost diurnal (Brunt et al., 2010; Padman et al., 2003). Therefore, small, solar-annual, or semi-annual (equinox) tides may drive the remaining variability in velocities observed at the GNSS sites that our model perturbations are unable to reproduce. Additionally, Mosbeux et al. (2023) observed a 6-month ~~tidal~~ signal in their GNSS datasets on the RIS and tentatively attributed this signal to semiannual changes in tides. This 6-month tidal signal may explain the observed intra-annual velocity variability at Site ~~4. However, Mosbeux et al. (2023) suggests this signal remains a source of noise in their interpretation of intra-annual ice shelf flow rather than a potential driver of ice flow variability . Additionally, significant ice velocity variations due to the diurnal tides of the Ross Sea occur on shorter timescales and closer to the calving front (Brunt et al., 2010; Makinson et al., 2011; Marsh et al., 2013).~~ 4, and we suggest that it is likely the tidal signal is playing a role in observed velocity variability at all GNSS sites.

Flow variability in the Siple Coast Ice Streams has also been shown to occur on short timescales due to changes in the distribution and supply of basal meltwater (Catania et al., 2012a). Recently, high basal melt rates of 35 m/a have been inferred

at the KIS grounding zone within a narrow subglacially sourced basal channel (Whiteford et al., 2022). These high basal melt rates within a subglacial channel suggest that meltwater plumes could be driving changes in the subglacial hydrology system of the KIS. These changes in the subglacial hydrology may be driving variations in the velocities on intra-annual timescales by modifying the basal friction at the KIS grounding line. However, further work is needed to investigate these observed intra-annual velocity variations at Site 4, which is outside the scope of this ~~paper~~study.

5 Conclusions

We tested the hypothesis that seasonal ~~variations~~ perturbations in basal melt can ~~explain~~ reproduce intra-annual velocity variability recorded at four long-duration GNSS stations on the Ross Ice Shelf (RIS) using ISSM. We presented three new GNSS datasets that display an intra-annual velocity variability (two velocity peaks per year) that has not yet been explored in previous studies (Klein et al., 2020; Mosbeux et al., 2023). We found that by perturbing basal melt rates at identified sensitive regions on the ice shelf we ~~were able to reproduce similar~~ can reproduce similar intra-annual velocity variations to the GNSS ~~intra-annual velocity variability at two of the GNSS stations. We suggest that seasonal changes in basal melt can explain the observed intra-annual velocity variability at~~ measurements at Sites 1 and ~~2. Our perturbed basal melt rates of 20 m/a on seasonal timescales at the calving front near the Ross Island pinning point are a likely scenario presently and in the future due to continued global warming (Stewart et al., 2019; Stevens et al., 2020; Das et al., 2020)~~2. We also show that seasonal variability in SSH alone cannot reproduce the intra-annual velocity variability observed at the new GNSS sites. However, ~~we suggest that seasonal changes in basal melting are unable to explain the observed intra-annual velocity variability at Sites 3 and 4. Site 3's modelled velocity variability displays significantly different phasing and magnitudes to the GNSS measurements. We find that the perturbed basal melt rates are unable to reproduce similar velocity variations to the GNSS measurements at Site 3. We~~ it is likely that changes in SSH and tides in the Ross Sea are contributing to the observed variability in velocities at all GNSS sites. We suggest that a combination of external forcings and internal mechanics may be at play to produce the observed intra-annual velocity variability at ~~Site~~ Sites 3 ~~, with recent work by Mosbeux et al. (2023) identifying that changes in SSH can explain this variability. Finally, we also suggest that seasonal changes in basal melt are unable to explain the observed intra-annual velocity variation at Site 4, with the unrealistic basal melt perturbation of 80 m/a needed to produce similar magnitudes in velocity variations. There have been no observations of seasonal changes in basal melt rates at the Siple Coast ice streams grounding lines, with the interior of the ice shelf experiencing much lower basal melt rates compared to the calving front (Horgan et al., 2011; Adusumilli et al., 2020; Smethie Jr and Jacobs, 2005).~~ and 4.

We suggest that ~~Site 4's observed intra-annual velocity variability is driven by a combination of external forcings and internal mechanics modifying the driving stresses and basal friction at the grounding line.~~

~~Future work should~~ future work could focus on (1) continuing and expanding the multi-year GNSS records of seasonally resolved ice velocity changes on the RIS, (2) ~~providing further understanding of the~~ examining ice shelf interactions with basal melt rates on floating and grounded ice through coupled ocean-ice shelf models, and (3) exploration of other potential drivers of intra-annual velocity variations particularly concerning the observed seasonal velocity variations at the KIS grounding zone.

Our results ~~can provide a further understanding of potential mechanisms driving the intra-annual velocity variations on the RIS~~highlight that seasonal perturbations in basal melt rates can reproduce GNSS-observed velocity variability in some cases, although the perturbations required in our study are large. The observed intra-annual velocity variations at all GNSS sites are likely driven by a complex combination of external forcings and internal mechanics on the RIS. However, our sensitivity maps highlight where increases in basal melt rates will influence ice velocity today and in the future. Specifically, the sensitive regions identified at the calving front near the Ross Island pinning point are already undergoing significant seasonal increases in basal melt rates (Stewart et al., 2019). Our AD-inferred sensitivity map shows that we do not need 20 m/a of perturbation under the entire ice shelf, but only over 2% of the ice shelf to reproduce the intra-annual velocity variations ~~.~~ at Sites 1 and 2. Therefore, we are likely to observe continued intra-annual velocity variations on the RIS driven by seasonal changes in basal melting at the calving front.

Appendix A

~~Locations where the basal melt rate is perturbed seasonally (i.e., where the AD mapped sensitivity is greater than $0.5e-11$ m^{-2} (highlighted in dark red)) for each GNSS site (green marker). The passive ice on the RIS identified by Fürst et al. (2016) is also outlined in black.~~
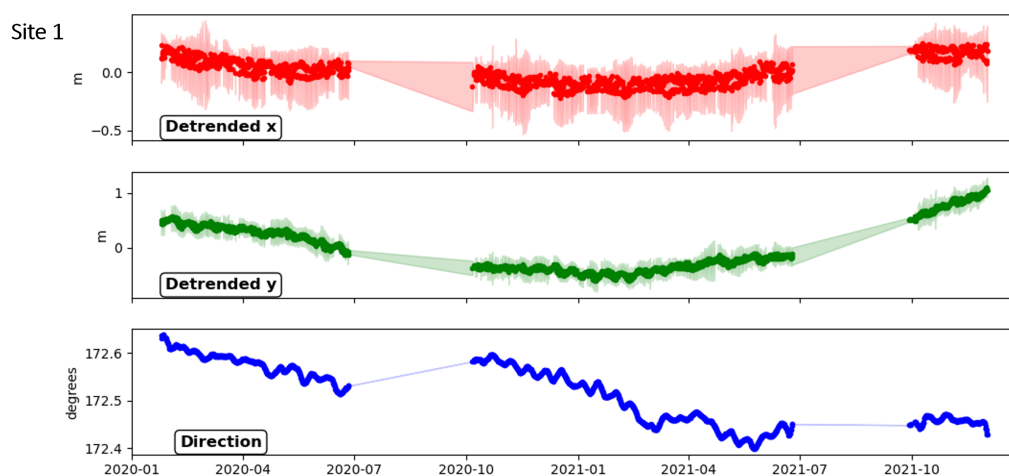
Figure A1. Site 1 GNSS detrended position (x, y) and direction (clockwise from ~~from~~ grid north).
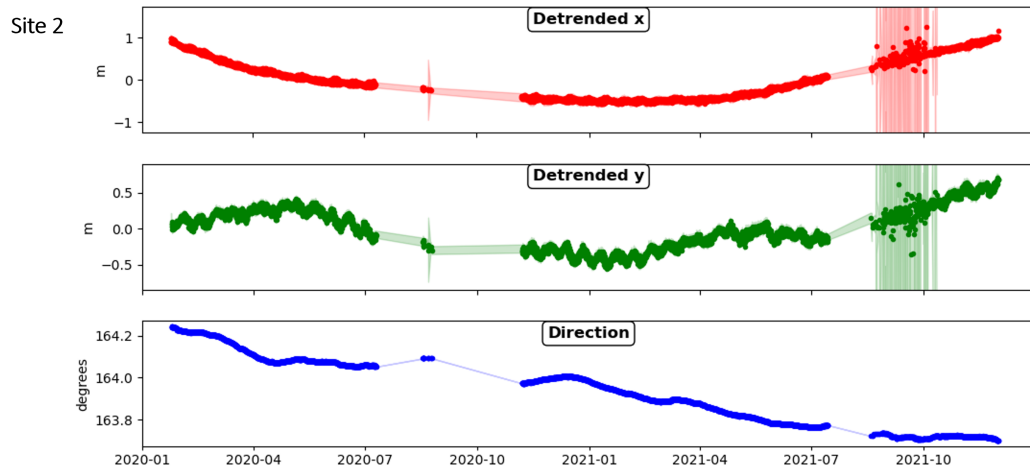
Figure A2. Site 2 GNSS detrended position (x, y) and direction (clockwise from from grid north).
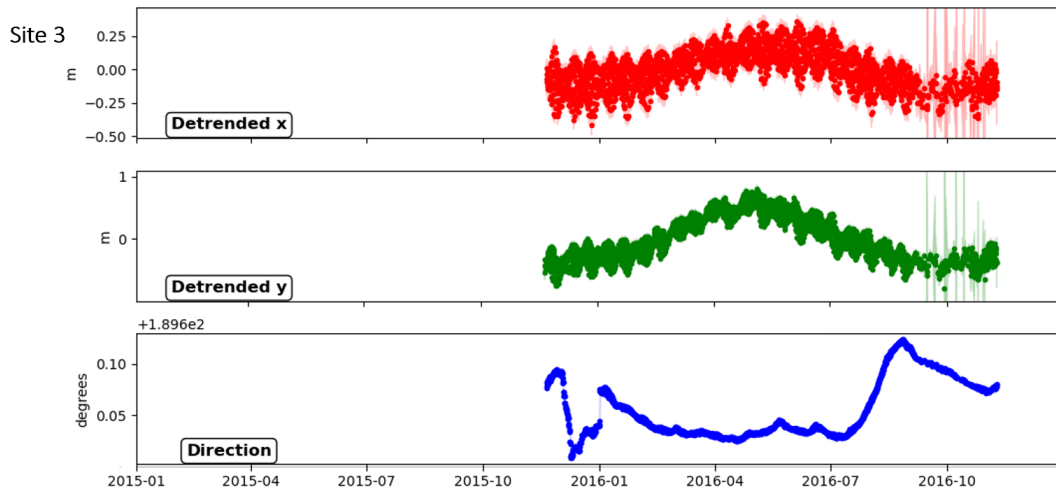
Figure A3. Site 3 GNSS detrended position (x, y) and direction (clockwise from ~~from~~ grid north).
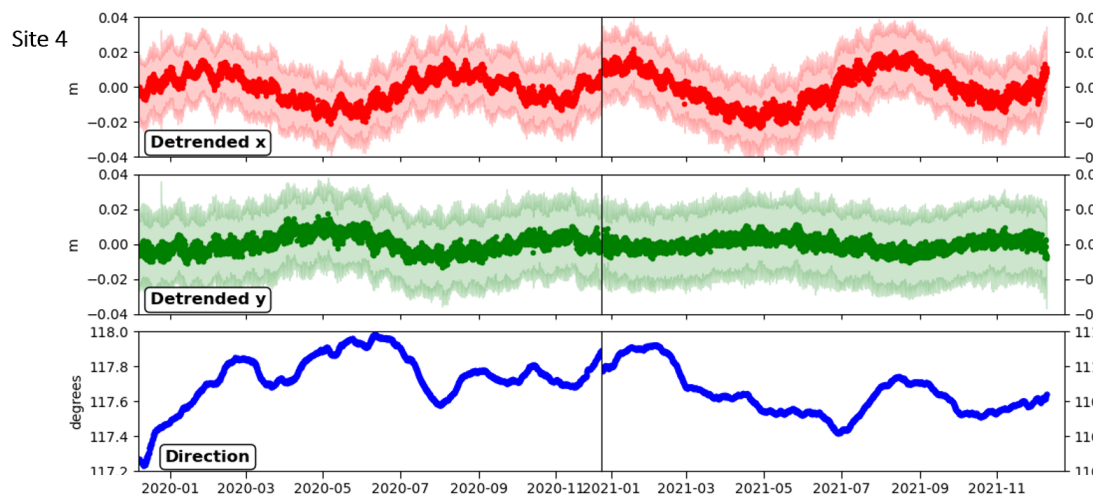
Figure A4. Site 4 GNSS detrended position (x, y) and direction (clockwise from from grid north).
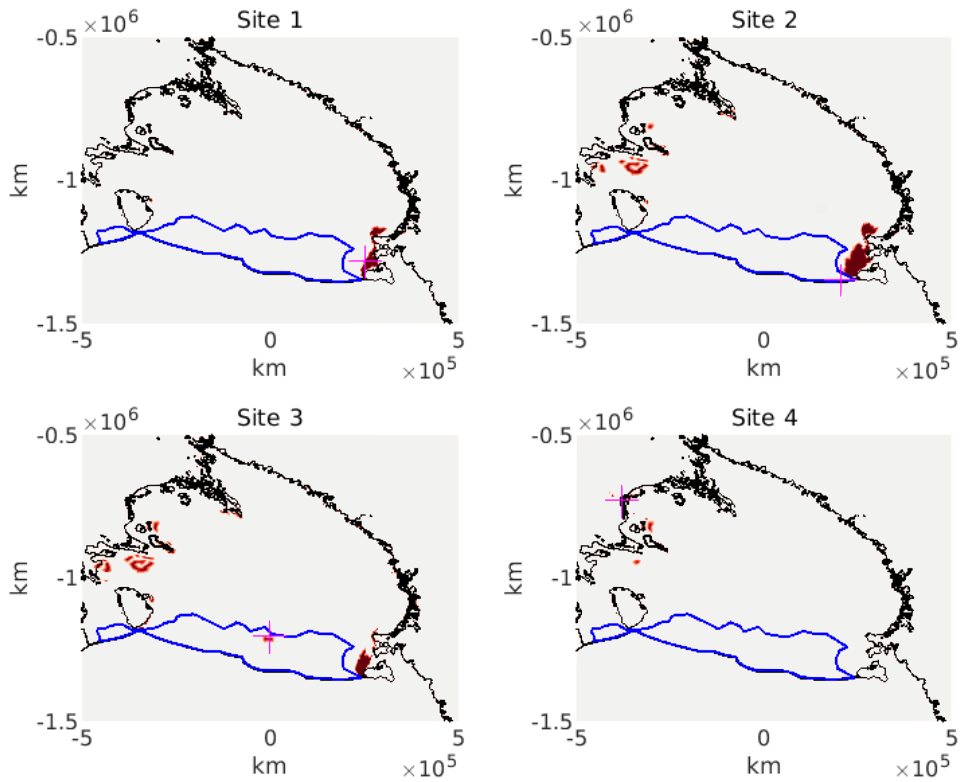
Figure A5. Locations where the basal melt rate was perturbed seasonally (i.e., where the AD mapped sensitivity is greater than $2e-11$ m^{-2} (dark red)) for each GNSS site (pink markers). The grounding line (black line) and passive ice (blue line) on the RIS identified by Fürst et al. (2016) are highlighted.
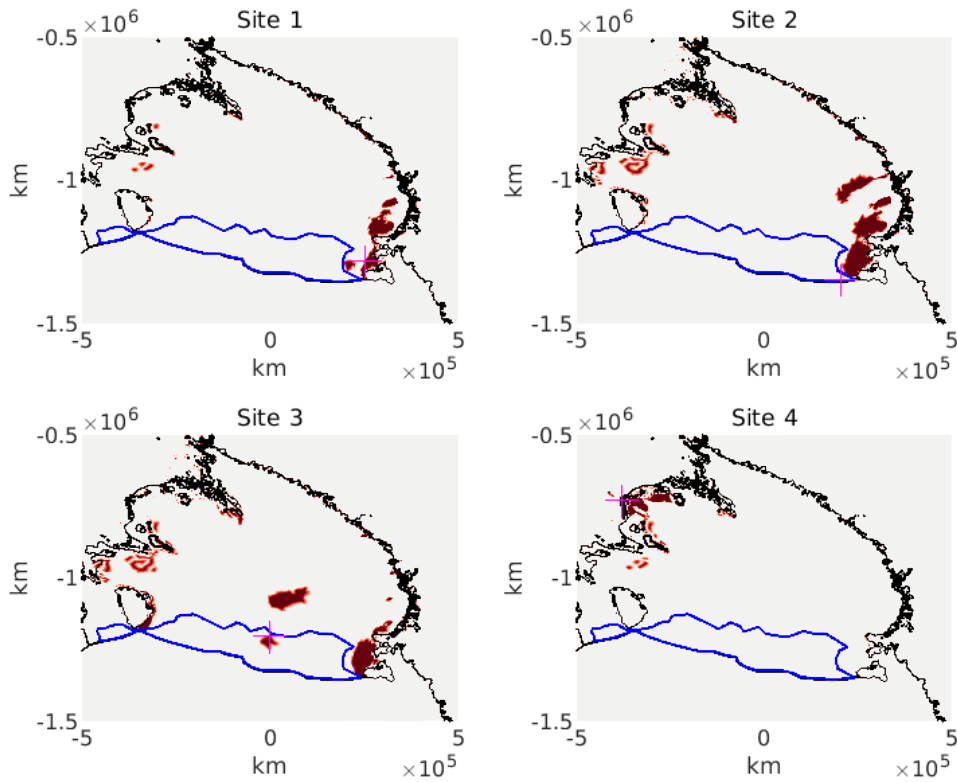
Figure A6. Locations where the basal melt rate is perturbed seasonally (i.e., where the AD mapped sensitivity is greater than $0.5e-11 \text{ m}^{-2}$ (highlighted in dark red)) for each GNSS site (pink marker). The grounding line (black line) and passive ice (blue line) on the RIS identified by Fürst et al. (2016) are highlighted.
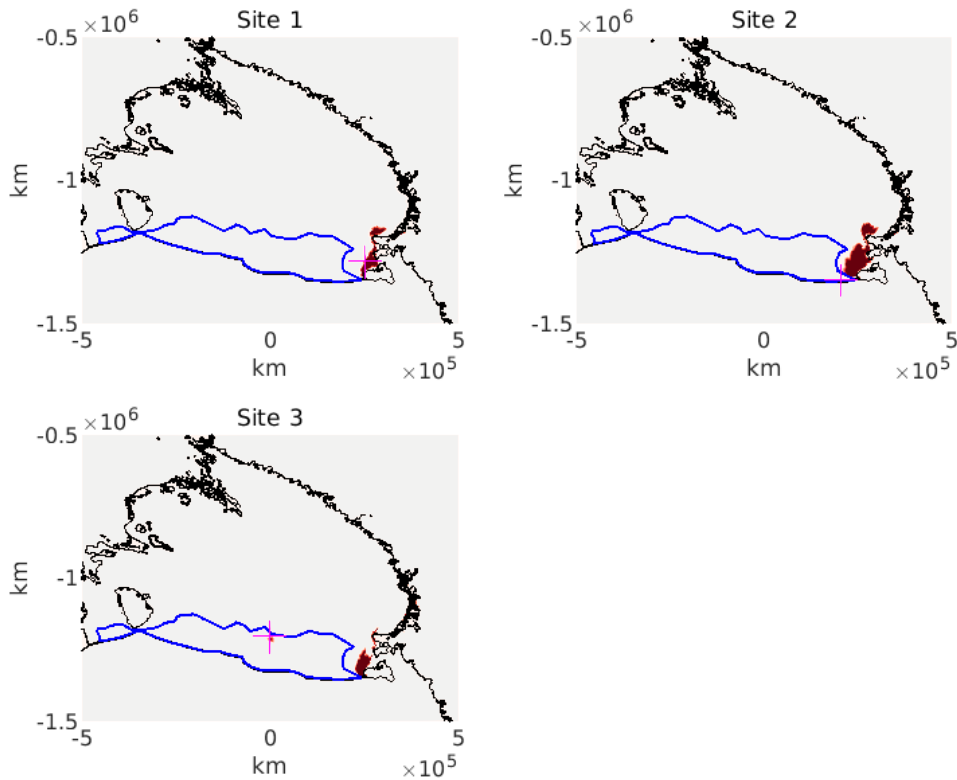
Figure A7. Locations where the basal melt rate is perturbed seasonally (i.e., where the AD mapped sensitivity is greater than $2e-11$ m^{-2} and located along the calving front close to the Ross Island pinning point (highlighted in dark red)) for GNSS Sites 1, 2 and 3 (pink marker). The grounding line (black line) and passive ice (blue line) on the RIS identified by Fürst et al. (2016) are highlighted.
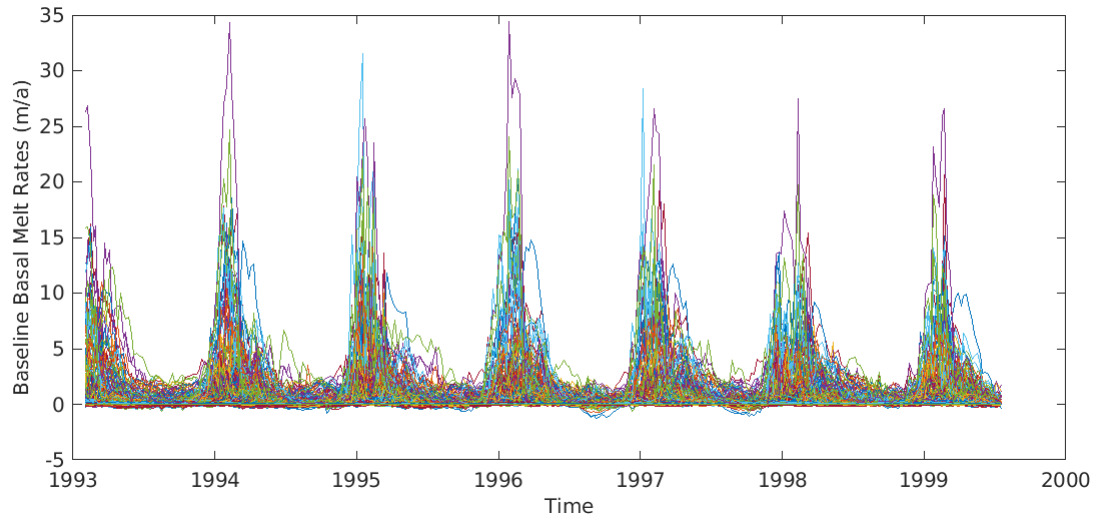
Figure A8. The baseline MITgcm basal melt rates for the identified sensitive regions (greater than $2e-11$ m^{-2}) on the RIS.
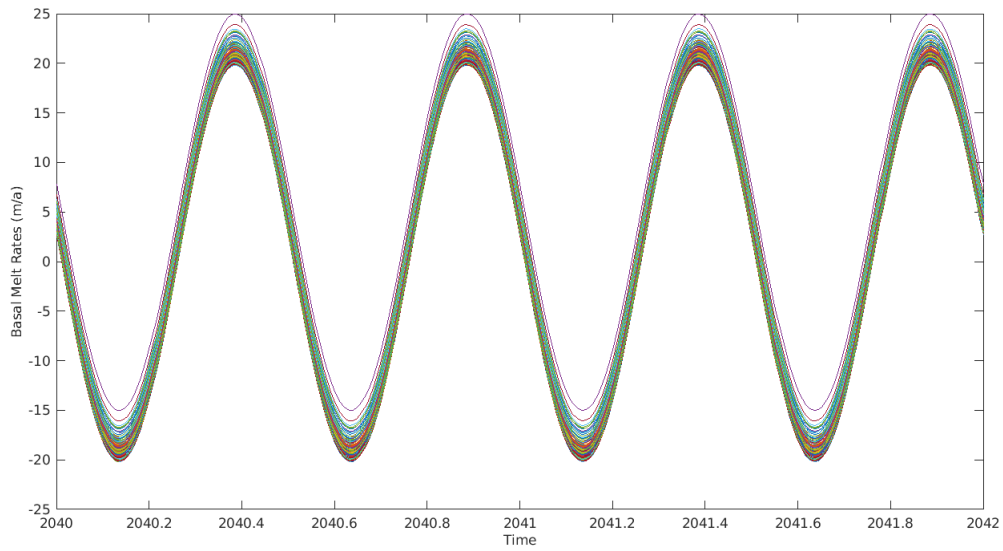
Figure A9. The perturbed MITgcm basal melt rates for the identified sensitive regions (greater than $2e-11$ m^{-2}) on the RIS.
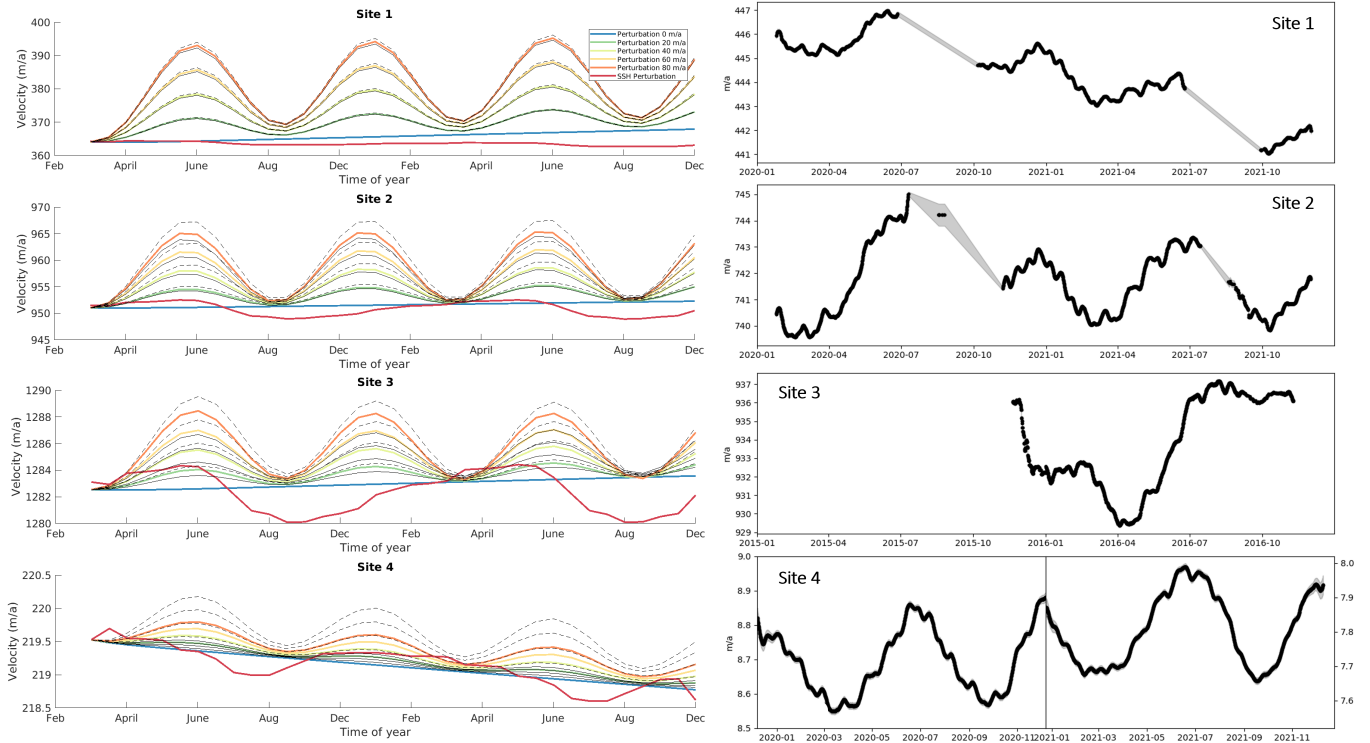
Figure A10. The absolute modelled velocities compared to the absolute GNSS observed velocities for Sites 1, 2, 3, and 4.

685 *Data availability.* The model scripts and configuration files used in this study can be found here https://doi.org/10.5281/zenodo.11098089. The Ice-sheet and Sea-level System Model v4.18 can be accessed at https://issm.jpl.nasa.gov. BedMachine Antarctica is available at NSIDC (http//nsidc.org/data/nsidc-0756). InSAR-Based ice velocity is found at NSIDC (https://nsidc.org/data/nsidc-0484/). The Antarctic surface mass balance (RACMO 2.3p2) is available at https://www.projects.science.uu.nl/iceclimate/models/racmo-data.php. GNSS data will be uploaded to a suitable repository (Zenodo) on acceptance.

690 *Author contributions.* Project vision, funding acquisition and field planning (2019/20 season) was led by Nicholas Golledge. The event leader for field season 2021/2022 was Alanna V. Alevropoulos-Borrill. Field assistants for fieldwork included Francesca Baldacchino, Laurine van Haastrecht, Dan Lowry, and Alexandra Gossart. Site 4 data acquisition and GNSS processing of all sites was carried out by Huw Horgan. GNSS analysis was carried out by Francesca Baldacchino and Huw Horgan. ISSM simulations and AD analysis were carried out by Francesca Baldacchino under the guidance of Mathieu Morlighem. AD simulations were carried out by Mathieu Morlighem. MITgcm basal melt outputs 695 were provided by Alena Malyarenko. All authors contributed to the manuscript.

Competing interests. Huw Horgan is an associate editor for The Cryosphere and EGUsphere. The authors declare that they have no other conflicts of interest.

Acknowledgements. We are grateful to Antarctic New Zealand for facilitating and supporting our field campaigns to the Ross Ice Shelf to install and collect GNSS measurements. Additionally, we are grateful to Peter Bromirski for sharing the raw GNSS datasets collected on the 700 Ross Ice Shelf in 2015-2016 that have been included in this ~~paper. Francesca Baldacchino thanks Laurie Padman for helpful correspondence early in this~~ study. This work was supported by the New Zealand Ministry for Business, Innovation and Employment contracts RTUV1705 ("NZSeaRise") and ANTA1801 ("Antarctic Science Platform"), and Royal Society of New Zealand contracts VUW-1501 and VUW16-02.

References

Adusumilli, S., Fricker, H. A., Medley, B., Padman, L., and Siegfried, M. R.: Interannual variations in meltwater input to the Southern Ocean from Antarctic ice shelves, Nature Geoscience, 13, 616–620, https://doi.org/10.1038/s41561-020-0616-z, 2020.

Agosta, C., Amory, C., Kittel, C., Orsi, A., Favier, V., Gallée, H., van den Broeke, M. R., Lenaerts, J. T. M., van Wessem, J. M., van de Berg, W. J., and Fettweis, X.: Estimation of the Antarctic surface mass balance using the regional climate model MAR (1979–2015) and identification of dominant processes, The Cryosphere, 13, 281–296, https://doi.org/10.5194/tc-13-281-2019, 2019.

Alley, K. E., Scambos, T. A., Anderson, R. S., Rajaram, H., Pope, A., and Haran, T. M.: Continent-wide estimates of Antarctic strain rates from Landsat 8-derived velocity grids, Journal of Glaciology, 64, 321–332, https://doi.org/10.1017/jog.2018.23, 2018.

Anandakrishnan, S., Voigt, D., Alley, R., and King, M.: Ice stream D flow speed is strongly modulated by the tide beneath the Ross Ice Shelf, Geophysical Research Letters, 30, 2003.

Anandakrishnan, S., Catania, G. A., Alley, R. B., and Horgan, H. J.: Discovery of till deposition at the grounding line of Whillans Ice Stream, Science, 315, 1835–1838, https://doi.org/10.1126/science.1138393, 2007.

Arndt, J. E., Larter, R. D., Friedl, P., Gohl, K., Höppner, K., et al.: Bathymetric controls on calving processes at Pine Island Glacier, The Cryosphere, 12, 2039–2050, 2018.

Årthun, M., Holland, P. R., Nicholls, K. W., and Feltham, D. L.: Eddy-driven exchange between the open ocean and a sub–ice shelf cavity, Journal of Physical Oceanography, 43, 2372–2387, 2013.

Assmann, K., Hellmer, H. H., and Beckmann, A.: Seasonal variation in circulation and water mass distribution on the Ross Sea continental shelf, Antarctic Science, 15, 3–11, https://doi.org/10.1017/S0954102003001007, 2003.

Baldacchino, F., Morlighem, M., Golledge, N. R., Horgan, H., and Malyarenko, A.: Sensitivity of the Ross Ice Shelf to environmental and glaciological controls, The Cryosphere, 16, 3723–3738, https://doi.org/10.5194/tc-16-3723-2022, 2022.

Bennett, M. R.: Ice streams as the arteries of an ice sheet: Their mechanics, stability and significance, Earth-Science Reviews, 61, 309–339, https://doi.org/10.1016/S0012-8252(02)00130-7, 2003.

Bindschadler, R. A., Vornberger, P. L., King, M. A., and Padman, L.: Tidally driven stick-slip motion in the mouth of Whillans Ice Stream, Antarctica, Annals of Glaciology, 36, 263–272, https://doi.org/10.3189/172756403781816284, 2003.

Bougamont, M., Christoffersen, P., Price, S., Fricker, H. A., Tulaczyk, S., and Carter, S. P.: Reactivation of Kamb Ice Stream tributaries triggers century-scale reorganization of Siple Coast ice flow in West Antarctica, Geophysical Research Letters, 42, 8471–8480, 2015.

Brunt, K. M.: Tidal motion of the Ross Ice Shelf and its interaction with the Siple Coast ice streams, Antarctica, The University of Chicago, 2008.

Brunt, K. M. and Macayeal, D. R.: Tidal modulation of ice-shelf flow: A viscous model of the Ross Ice Shelf, Journal of Glaciology, 60, 500–508, https://doi.org/10.3189/2014JoG13J203, 2014.

Brunt, K. M., King, M. A., Fricker, H. A., and MacAyeal, D. R.: Flow of the Ross Ice Shelf, Antarctica, is modulated by the ocean tide, Journal of Glaciology, 56, 157–161, https://doi.org/10.3189/002214310791190875, 2010.

Campbell, A. J., Hulbe, C. L., and Lee, C. K.: Ice Stream Slowdown Will Drive Long-Term Thinning of the Ross Ice Shelf, With or Without Ocean Warming, Geophysical Research Letters, 45, 201–206, https://doi.org/10.1002/2017GL075794, 2018.

Cassotto, R., Fahnestock, M., Amundson, J. M., Truffer, M., and Joughin, I.: Seasonal and interannual variations in ice melange and its impact on terminus stability, Jakobshavn Isbræ, Greenland, Journal of Glaciology, 61, 76–88, https://doi.org/10.3189/2015JoG13J235, 2015.

740 Catania, G., Hulbe, C., Conway, H., Scambos, T. A., and Raymond, C.: Variability in the mass flux of the Ross ice streams, West Antarctica, over the last millennium, Journal of Glaciology, 58, 741–752, 2012a.

Catania, G., Hulbe, C., Conway, H., Scambos, T. A., and Raymond, C. F.: Variability in the mass flux of the Ross ice streams, West Antarctica, over the last millennium, Journal of Glaciology, 58, 741–752, https://doi.org/10.3189/2012JoG11J219, 2012b.

Cavanagh, J., Lampkin, D., and Moon, T.: Seasonal variability in regional ice flow due to meltwater injection into the shear margins of
745 Jakobshavn Isbræ, Journal of Geophysical Research: Earth Surface, 122, 2488–2505, 2017.

Chaput, J., Aster, R., McGrath, D., Baker, M., Anthony, R. E., Gerstoft, P., Bromirski, P., Nyblade, A., Stephen, R., Wiens, D., et al.: Near-surface environmentally forced changes in the Ross Ice Shelf observed with ambient seismic noise, Geophysical Research Letters, 45, 11–187, 2018.

Christianson, K., Bushuk, M., Dutrieux, P., Parizek, B. R., Joughin, I. R., Alley, R. B., Shean, D. E., Abrahamsen, E. P., Anandakrishnan, S.,
750 Heywood, K. J., et al.: Sensitivity of Pine Island Glacier to observed ocean forcing, Geophysical Research Letters, 43, 10–817, 2016.

Clem, K. R., Orr, A., and Pope, J. O.: The Springtime Influence of Natural Tropical Pacific Variability on the Surface Climate of the Ross Ice Shelf, West Antarctica: Implications for Ice Shelf Thinning, Scientific Reports, 8, 1–10, https://doi.org/10.1038/s41598-018-30496-5, 2018.

Cuffey, K. M. and Paterson, W. S. B.: The physics of glaciers, Academic Press, 2010.

755 Das, I., Padman, L., Bell, R. E., Fricker, H. A., Tinto, K. J., Hulbe, C. L., Siddoway, C. S., Dhakal, T., Frearson, N. P., Mosbeux, C., Cordero, S. I., and Siegfried, M. R.: Multidecadal Basal Melt Rates and Structure of the Ross Ice Shelf, Antarctica, Using Airborne Ice Penetrating Radar, Journal of Geophysical Research: Earth Surface, 125, https://doi.org/10.1029/2019JF005241, 2020.

Davis, P. and Nicholls, K.: Turbulence observations beneath Larsen C Ice Shelf, Antarctica., J. Geophys. Res, 124, 5529–5550, https://doi.org/10.1029/2019jc015164, 2019.

760 Depoorter, M. A., Bamber, J. L., Griggs, J. A., Lenaerts, J. T., Ligtenberg, S. R., Van Den Broeke, M. R., and Moholdt, G.: Calving fluxes and basal melt rates of Antarctic ice shelves, Nature, 502, 89–92, https://doi.org/10.1038/nature12567, 2013.

Dinniman, Asay-Davis, X. S., Galton-Fenzi, B. K., Holland, P. R., Jenkins, A., and Timmermann, R.: Modeling ice shelf/ocean interaction in Antarctica: A review, https://doi.org/10.5670/oceanog.2016.106, 2016.

Dinniman, M., Klinck, J., Hofmann, E., and Smith, W.: Effects of Projected Changes in Wind, Atmospheric Temperature, and Freshwater
765 Inflow on the Ross Sea, Journal of Climate, 31, 90–103, https://doi.org/10.1175/JCLI-D-17-0351.1, 2018.

Dirscherl, M., Dietz, A. J., Dech, S., and Kuenzer, C.: Remote sensing of ice motion in Antarctica – A review, Remote Sensing of Environment, 237, 111 595, https://doi.org/10.1016/j.rse.2019.111595, 2020.

Dupond, T. and Alley, R.: Assessment of the importance of ice-shelf buttressing to ice-sheet flow., Journal of Geophysical Research Letters, 32, 2005.

770 Dutrieux, P., De Rydt, J., Jenkins, A., Holland, P. R., Ha, H. K., Lee, S. H., Steig, E. J., Ding, Q., Abrahamsen, E. P., and Schröder, M.: Strong sensitivity of pine Island ice-shelf melting to climatic variability, Science, 343, 174–178, https://doi.org/10.1126/science.1244341, 2014.

Feldmann, J., Reese, R., Winkelmann, R., and Levermann, A.: Shear-margin melting causes stronger transient ice discharge than ice-stream melting in idealized simulations., The Cryosphere, 16, 1927–1940, https://doi.org/10.5194/tc-16-1927-2022, 2022.

775 Fürst, J. J., Durand, G., Gillet-Chaulet, F., Tavard, L., Rankl, M., Braun, M., and Gagliardini, O.: The safety band of Antarctic ice shelves, Nature Climate Change, 6, 479–482, https://doi.org/10.1038/nclimate2912, 2016.

Gagliardini, O., Durand, G., Zwinger, T., Hindmarsh, R. C., and Le Meur, E.: Coupling of ice-shelf melting and buttressing is a key process in ice-sheets dynamics, Geophysical Research Letters, 37, 1–5, https://doi.org/10.1029/2010GL043334, 2010.

Greene, C. A., Gwyther, D. E., and Blankenship, D. D.: Antarctic Mapping Tools for MATLAB, Computers and Geosciences, 104, 151–157, https://doi.org/10.1016/j.cageo.2016.08.003, 2017.

Greene, C. A., Young, D. A., Gwyther, D. E., Galton-fenzi, B. K., and Blankenship, D. D.: Seasonal dynamics of Totten Ice Shelf controlled by sea ice buttressing, 12, 2869–2882, 2018.

Greene, C. A., Gardner, A. S., Schlegel, N.-J., and Fraser, A. D.: Antarctic calving loss rivals ice-shelf thinning, Nature, 609, 948–953, 2022.

Gudmundsson, G.: Fortnightly variations in the flow velocity of Rutford Ice Stream, West Antarctica, Nature, 444, 1063–1064, https://doi.org/10.1038/nature05430, 2006.

Gudmundsson, G. H.: Ice-shelf buttressing and the stability of marine ice sheets, Cryosphere, 7, 647–655, https://doi.org/10.5194/tc-7-647-2013, 2013.

Gudmundsson, G. H., Paolo, F. S., Adusumilli, S., and Fricker, H. A.: Instantaneous Antarctic Ice Sheet mass loss driven by thinning ice shelves, Geophysical Research Letters, 46, 13 903–13 909, 2019.

Holland, D. and Jenkins, A.: Modeling Thermodynamic Ice–Ocean Interactions at the Base of an Ice Shelf., Journal of Physical Oceanography, 29, 1787–1800, https://doi.org/10.1175/1520-0485, 1999.

Holland, D. M., Jacobs, S. S., and Jenkins, A.: Modelling the ocean circulation beneath the Ross Ice Shelf, Antarctic Science, 15, 13–23, 2003.

Horgan, H. J., Walker, R. T., Anandakrishnan, S., and Alley, R. B.: Surface elevation changes at the front of the Ross Ice Shelf: Implications for basal melting, Journal of Geophysical Research: Oceans, 116, 1–12, https://doi.org/10.1029/2010JC006192, 2011.

Horgan, H. J., van Haastrecht, L., Alley, R. B., Anandakrishnan, S., Beem, L. H., Christianson, K., Muto, A., and Siegfried, M. R.: Grounding zone subglacial properties from calibrated active-source seismic methods, The Cryosphere, 15, 1863–1880, https://doi.org/10.5194/tc-15-1863-2021, 2021.

Howat, I. M., Box, J. E., Ahn, Y., Herrington, A., and McFadden, E. M.: Seasonal variability in the dynamics of marine-terminating outlet glaciers in Greenland, Journal of Glaciology, 56, 601–613, https://doi.org/10.3189/002214310793146232, 2010.

Hulbe, C., Scambos, T., Klinger, M., and Fahnestock, M.: Flow variability and ongoing margin shifts on Bindschadler and MacAyeal Ice Streams, West Antarctica, Journal of Geophysical Rsearch, Earth Surface, 121, 283–293, https://doi.org/10.1002/2015JF003670, 2016.

Hulbe, C. L., Scambos, T. A., Lee, C. K., Bohlander, J., and Haran, T.: Recent changes in the flow of the Ross Ice Shelf, West Antarctica, Earth and Planetary Science Letters, 376, 54–62, https://doi.org/10.1016/j.epsl.2013.06.013, 2013.

Jacobs, S., Helmer, H., Doake, C., Jenkins, A., and Frolich, R.: Melting of ice shelves and the mass balance of Antarctica, Journal of Glaciology, 38, 375–387, 1992.

Jendersie, S., Williams, M. J. M., Langhorne, P. J., and Robertson, R.: The Density-Driven Winter Intensification of the Ross Sea Circulation, Journal of Geophysical Research: Oceans, 123, 7702–7724, https://doi.org/10.1029/2018JC013965, 2018.

Jenkins, A., Shoosmith, D., Dutrieux, P., Jacobs, S., Kim, T. W., Lee, S. H., Ha, H. K., and Stammerjohn, S.: West Antarctic Ice Sheet retreat in the Amundsen Sea driven by decadal oceanic variability, Nature Geoscience, 11, 733–738, https://doi.org/10.1038/s41561-018-0207-4, 2018.

Joughin, Smith, B. E., and Medley, B.: Marine ice sheet collapse potentially under way for the Thwaites Glacier Basin, West Antarctica, Science, 344, 735–738, 2014.

Joughin, I., MacAyeal, D. R., and Tulaczyk, S.: Basal shear stress of the Ross ice streams from control method inversions, Journal of Geophysical Research: Solid Earth, 109, 1–20, https://doi.org/10.1029/2003JB002960, 2004.

Joughin, I., Alley, R. B., and Holland, D. M.: Oceanic Forcing, Science, 338, 1172–6, https://doi.org/10.1126/science.1226481, 2013.

Joughin, I., Shapero, D., Smith, B., Dutrieux, P., and Barham, M.: Ice-shelf retreat drives recent Pine Island Glacier speedup, Science Advances, 7, eabg3080, 2021.

Kamb, B.: Rheological nonlinearity and flow instability in the deforming bed mechanism of ice stream motion, Journal of Geophysical Research: Solid Earth, 96, 16 585–16 595, 1991.

King, M., Makinson, K., and Gudmundsson, G. H.: Nonlinear interaction between ocean tides and the Larsen C Ice Shelf system, Geophysical Research Letters, 38, 1–5, https://doi.org/10.1029/2011GL046680, 2011.

Klein, E., Mosbeux, C., Bromirski, P. D., Padman, L., Bock, Y., Springer, S. R., and Fricker, H. A.: Annual cycle in flow of Ross Ice Shelf, Antarctica: Contribution of variable basal melting, Journal of Glaciology, 66, 861–875, https://doi.org/10.1017/jog.2020.61, 2020.

Larter, R. D.: Basal Melting, Roughness and Structural Integrity of Ice Shelves, Geophysical Research Letters, 49, e2021GL097 421, https://doi.org/10.1029/2021GL097421, 2022.

Lhermitte, S., Sun, S., Shuman, C., Wouters, B., Pattyn, F., Wuite, J., Berthier, E., and Nagler, T.: Damage accelerates ice shelf instability and mass loss in Amundsen Sea Embayment, Proceedings of the National Academy of Sciences of the United States of America, 117, 24 735–24 741, https://doi.org/10.1073/pnas.1912890117, 2020.

Lipscomb, W. H., Leguy, G. R., Jourdain, N. C., Asay-Davis, X., Seroussi, H., and Nowicki, S.: ISMIP6-based projections of ocean-forced Antarctic Ice Sheet evolution using the Community Ice Sheet Model, The Cryosphere, 15, 633–661, 2021.

Liu, H. and Miller, K.: Fracture toughness of fresh-water ice, Journal of glaciology, 22, 135–143, 1979.

Losch, M.: Modeling ice shelf cavities in a z coordinate ocean general circulation model, Journal of Geophysical Research: Oceans (1978–2012), 113, https://doi.org/10.1029/2007jc004368, 2008.

MacAyeal, D. R.: Irregular oscillations of the West Antarctic ice sheet, Nature, 359, 29–32, 1992.

Makinson, K., Holland, P. R., Nicholls, K. W., and Holland, D. M.: Influence of tides on melting and freezing beneath Filchner-Ronne Ice Shelf, Antarctica, Geophysical Research Letters, 38, https://doi.org/10.1029/2010GL046462, 2011.

Malyarenko, A., Robinson, N. J., Williams, M. J. M., and Langhorne, P. J.: A Wedge Mechanism for Summer Surface Water Inflow Into the Ross Ice Shelf Cavity, Journal of Geophysical Research: Oceans, 124, 1196–1214, https://doi.org/10.1029/2018jc014594, 2019.

Marsh, O. J., Rack, W., Floricioiu, D., Golledge, N. R., and Lawson, W.: Tidally induced velocity variations of the beardmore glacier, Antarctica, and their representation in satellite measurements of ice velocity, Cryosphere, 7, 1375–1384, https://doi.org/10.5194/tc-7-1375-2013, 2013.

Marsh, O. J., Fricker, H. A., Siegfried, M. R., Christianson, K., Nicholls, K. W., Corr, H. F., and Catania, G.: High basal melting forming a channel at the grounding line of Ross Ice Shelf, Antarctica, Geophysical Research Letters, 43, 250–255, https://doi.org/10.1002/2015GL066612, 2016.

Matsuoka, K., Hindmarsh, R. C., Moholdt, G., Bentley, M. J., Pritchard, H. D., Brown, J., Conway, H., Drews, R., Durand, G., Goldberg, D., Hattermann, T., Kingslake, J., Lenaerts, J. T., Martín, C., Mulvaney, R., Nicholls, K. W., Pattyn, F., Ross, N., Scambos, T., and Whitehouse, P. L.: Antarctic ice rises and rumples: Their properties and significance for ice-sheet dynamics and evolution, Earth-Science Reviews, 150, 724–745, https://doi.org/10.1016/j.earscirev.2015.09.004, 2015.

Michel, R., Linick, T., and Williams, P.: Tritium and carbon-14 distributions in seawater from under the Ross Ice Shelf Project ice hole, Science, 203, 445–446, 1979.

Moholdt, G., Padman, L., and Fricker, H. A.: Basal mass budget of Ross and Filchner-Ronne ice shelves, Antarctica, derived from Lagrangian analysis of ICESat altimetry, Journal of Geophysical Research: Earth Surface, 119, 2361–2380, https://doi.org/10.1002/2014JF003171, 2014.

855 Morlighem, M., Rignot, E., Seroussi, H., Larour, E., Ben Dhia, H., and Aubry, D.: Spatial patterns of basal drag inferred using control methods from a full-Stokes and simpler models for Pine Island Glacier, West Antarctica, Geophysical Research Letters, 37, 1–6, https://doi.org/10.1029/2010GL043853, 2010.

Morlighem, M., Seroussi, H., Larour, E., and Rignot, E.: Inversion of basal friction in Antarctica using exact and incomplete adjoints of a higher-order model, Journal of Geophysical Research: Earth Surface, 118, 1746–1753, https://doi.org/10.1002/jgrf.20125, 2013.

860 Mosbeux, C., Padman, L., Klein, E., Bromirski, P., and Fricker, H.: Seasonal variability in Antarctic ice shelf velocities forced by sea surface height variations, The Cryosphere, 17, 2585–2606, 2023.

Mottram, R., Simonsen, S. B., Svendsen, S. H., Barletta, V. R., Sørensen, L. S., Nagler, T., Wuite, J., Groh, A., Horwath, M., Rosier, J., Solgaard, A., Hvidberg, C. S., and Forsberg, R.: An integrated view of Greenland Ice Sheet mass changes based on models and satellite observations, Remote Sensing, 11, 1–26, https://doi.org/10.3390/rs11121407, 2019.

865 Murray, T., Smith, A., King, M., and Weedon, G.: Ice flow modulated by tides at up to annual periods at Rutford Ice Stream, West Antarctica, Geophysical Research Letters, 34, 2007.

Nakayama, Y., Manucharyan, G., Zhang, H., Dutrieux, P., Torres, H. S., Klein, P., Seroussi, H., Schodlok, M., Rignot, E., and Menemenlis, D.: Pathways of ocean heat towards Pine Island and Thwaites grounding lines, Scientific reports, 9, 16 649, 2019.

Ng, F. and Conway, H.: Fast-flow signature in the stagnated Kamb Ice Stream, West Antarctica, Geology, 32, 481–484, 2004.

870 Nicolas, J. P., Vogelmann, A. M., Scott, R. C., Wilson, A. B., Cadeddu, M. P., Bromwich, D. H., Verlinde, J., Lubin, D., Russell, L. M., Jenkinson, C., et al.: January 2016 extensive summer melt in West Antarctica favoured by strong El Niño, Nature communications, 8, 1–10, 2017a.

Nicolas, J. P., Vogelmann, A. M., Scott, R. C., Wilson, A. B., Cadeddu, M. P., Bromwich, D. H., Verlinde, J., Lubin, D., Russell, L. M., Jenkinson, C., et al.: January 2016 extensive summer melt in West Antarctica favoured by strong El Niño, Nature communications, 8,
875 15 799, 2017b.

Padman, L., Erofeeva, S., and Joughin, I.: Tides of the Ross Sea and Ross Ice Shelf cavity, Antarctic Science, 15, 31–40, https://doi.org/10.1017/S0954102003001032, 2003.

Paolo, F., Padman, L., Fricker, H., Adusumilli, S., Howard, S., and Siegfried, M.: Response of Pacific-sector Antarctic ice shelves to the El Niño/Southern oscillation, Nature geoscience, 11, 121–126, 2018.

880 Paolo, F. S., Fricker, H. A., and Padman, L.: Volume loss from Antarctic ice shelves is accelerating, Science, 348, 327–331, https://doi.org/10.1126/science.aaa0940, 2015.

Pattyn, F.: Sea-level response to melting of Antarctic ice shelves on multi-centennial timescales with the fast Elementary Thermomechanical Ice Sheet model (f.ETISh v1.0), Cryosphere, 11, 1851–1878, https://doi.org/10.5194/tc-11-1851-2017, 2017.

Pattyn, F. and Durand, G.: Why marine ice sheet model predictions may diverge in estimating future sea level rise, Geophysical Research
885 Letters, 40, 4316–4320, https://doi.org/10.1002/grl.50824, 2013.

Pattyn, F., Ritz, C., Hanna, E., Asay-Davis, X., DeConto, R., Durand, G., Favier, L., Fettweis, X., Goelzer, H., Golledge, N. R., Kuipers Munneke, P., Lenaerts, J. T., Nowicki, S., Payne, A. J., Robinson, A., Seroussi, H., Trusel, L. D., and van den Broeke, M.: The Greenland and Antarctic Ice Sheets under 1.5 °C global warming, Nature Climate Change, 8, 1053–1061, https://doi.org/10.1038/s41558-018-0305-8, 2018.

890 Porter, D. F., Springer, S. R., Padman, L., Fricker, H. A., Tinto, K. J., Riser, S. C., and Bell, R. E.: Evolution of the Seasonal Surface Mixed Layer of the Ross Sea, Antarctica, Observed With Autonomous Profiling Floats, Journal of Geophysical Research: Oceans, 124, 4934–4953, https://doi.org/10.1029/2018JC014683, 2019.

Ranganathan, M., Minchew, B., Meyer, C. R., and Gudmundsson, G. H.: A new approach to inferring basal drag and ice rheology in ice streams, with applications to West Antarctic Ice Streams, Journal of Glaciology, 67, 229–242, https://doi.org/10.1017/jog.2020.95, 2021.

895 Ray, R. D., Larson, K. M., and Haines, B. J.: New determinations of tides on the north-western Ross Ice Shelf., Antarctic Science, 33, 89–102, https://doi.org/10.1017/S0954102020000498, 2021.

Reddy, T. E., Arrigo, K. R., and Holland, D. M.: The role of thermal and mechanical processes in the formation of the Ross Sea summer polynya, Journal of Geophysical Research: Oceans, 112, 2007.

Reddy, T. E., Holland, D. M., and Arrigo, K. R.: Ross ice shelf cavity circulation, residence time, and melting: Results from a model of
900 oceanic chlorofluorocarbons, Continental Shelf Research, 30, 733–742, 2010.

Reese, R., Gudmundsson, G. H., Levermann, A., and Winkelmann, R.: The far reach of ice-shelf thinning in Antarctica, Nature Climate Change, 8, 53–57, https://doi.org/10.1038/s41558-017-0020-x, 2018.

Retzlaff, R. and Bentley, C. R.: Timing of stagnation of Ice Stream C, West Antarctica, from short-pulse radar studies of buried surface crevasses, Journal of Glaciology, 39, 553–561, 1993.

905 Rignot, Jacobs, S., Mouginot, J., and Scheuchl, B.: Ice-shelf melting around Antarctica, Science, 341, 266–270, https://doi.org/10.1126/science.1235798, 2013.

Rignot, Mouginot, and B, S.: MEaSUREs INSAR-Based Antarctica Ice Velocity Map, Version 2, Boulder, Colorado USA. NASA National Snow and Ice Data Center Distributed Active Archive Center, https://doi.org/10.5067/D7GK8F5J8M8R, accessed on 20/02/2020, 2017.

Rignot, E., Mouginot, J., Scheuchl, B., van den Broeke, M., van Wessem, M. J., and Morlighem., M.: Four decades of Antarctic Ice Sheet mass
910 balance from 1979-2017, Proceedings of the National Academy of Sciences, 116, 1095–1103, https://doi.org/10.1073/pnas.1812883116, 2019.

Roberts, J., Galton-Fenzi, B. K., Paolo, F. S., Donnelly, C., Gwyther, D. E., Padman, L., Young, D., Warner, R., Greenbaum, J., Fricker, H. A., et al.: Ocean forced variability of Totten Glacier mass loss, Geological Society, London, Special Publications, 461, 175–186, 2018.

Rosier, S. H. and Gudmundsson, G. H.: Exploring mechanisms responsible for tidal modulation in flow of the Filchner-Ronne Ice Shelf,
915 Cryosphere, 14, 17–37, https://doi.org/10.5194/tc-14-17-2020, 2020.

Sagebaum, M., Albring, T., and Gauger., N.: High-Performance Derivative Computations using CoDiPack, ACM Transactions on Mathematical Software (TOMS), 45, https://dl.acm.org/doi/abs/10.1145/3356900, 2019.

Schlegel, N. J., Seroussi, H., Schodlok, M. P., Larour, E. Y., Boening, C., Limonadi, D., Watkins, M. M., Morlighem, M., and Van Den Broeke, M. R.: Exploration of Antarctic Ice Sheet 100-year contribution to sea level rise and associated model uncertainties using the
920 ISSM framework, Cryosphere, 12, 3511–3534, https://doi.org/10.5194/tc-12-3511-2018, 2018.

Schodlok, M., Menemenlis, D., and Rignot, E.: Ice shelf basal melt rates around Antarctica from simulations and observations., Journal of Geophysical Research, 121, 1085–1109, https://doi.org/10.1002/2015JC011117, 2016.

Schoof, C.: Ice sheet grounding line dynamics: Steady states, stability, and hysteresis, Journal of Geophysical Research: Earth Surface, 112, 1–19, https://doi.org/10.1029/2006JF000664, 2007.

925 Shabtaie, S. and Bentley, C.: West Antarctic ice streams draining into the Ross Ice Shelf: configuration and mass balance., Journal of Geophysical Research, 92, 1311–1336, https://doi.org/10.1029/JB092iB02p01311, 1987.

Shepherd, A., Wingham, D., and Rignot, E.: Warm ocean is eroding West Antarctic ice sheet, Geophysical Research Letters, 31, 2004.

Shepherd, A., Ivins, E. R., Geruo, A., Barletta, V. R., Bentley, M. J., Bettadpur, S., Briggs, K. H., Bromwich, D. H., Forsberg, R., Galin, N., Horwath, M., Jacobs, S., Joughin, I., King, M. A., Lenaerts, J. T., Li, J., Ligtenberg, S. R., Luckman, A., Luthcke, S. B., McMillan, M., Meister, R., Milne, G., Mouginot, J., Muir, A., Nicolas, J. P., Paden, J., Payne, A. J., Pritchard, H., Rignot, E., Rott, H., Sørensen, L. S., Scambos, T. A., Scheuchl, B., Schrama, E. J., Smith, B., Sundal, A. V., Van Angelen, J. H., Van De Berg, W. J., Van Den Broeke, M. R., Vaughan, D. G., Velicogna, I., Wahr, J., Whitehouse, P. L., Wingham, D. J., Yi, D., Young, D., and Zwally, H. J.: A reconciled estimate of ice-sheet mass balance, Science, 338, 1183–1189, https://doi.org/10.1126/science.1228102, 2012.

Shepherd, A., Fricker, H. A., and Farrell, S. L.: Trends and connections across the Antarctic cryosphere, Nature, 558, 223–232, https://doi.org/10.1038/s41586-018-0171-6, 2018.

Smethie Jr, W. M. and Jacobs, S. S.: Circulation and melting under the Ross Ice Shelf: estimates from evolving CFC, salinity and temperature fields in the Ross Sea, Deep Sea Research Part I: Oceanographic Research Papers, 52, 959–978, 2005.

Smith, B., Fricker, H. A., Gardner, A. S., Medley, B., Nilsson, J., Paolo, F. S., Holschuh, N., Adusumilli, S., Brunt, K., Csatho, B., et al.: Pervasive ice sheet mass loss reflects competing ocean and atmosphere processes, Science, 368, 1239–1242, 2020.

Smith Jr., W. O., Dinniman, M. S., Hofmann, E. E., and Klinck, J. M.: The effects of changing winds and temperatures on the oceanography of the Ross Sea in the 21st century, Geophysical Research Letters, 41, 1624–1631, https://doi.org/10.1002/2014GL059311, 2014.

Stearns., L., Smith, B. E., and Hamilton, G. S.: Increased flow speed on a large east antarctic outlet glacier caused by subglacial floods, Nature Geoscience, 1, 827–831, https://doi.org/10.1038/ngeo356, 2008.

Stern, A. A., Dinniman, M. S., Zagorodnov, V., Tyler, S. W., and Holland, D. M.: Intrusion of warm surface water beneath the McMurdo ice shelf, Antarctica, Journal of Geophysical Research: Oceans, 118, 7036–7048, https://doi.org/10.1002/2013JC008842, 2013.

Stevens, C., Hulbe, C., Brewer, M., Stewart, C., Robinson, N., Ohneiser, C., and Jendersie, S.: Ocean mixing and heat transport processes observed under the Ross Ice Shelf control its basal melting, Proceedings of the National Academy of Sciences of the United States of America, 117, 16 799–16 804, https://doi.org/10.1073/pnas.1910760117, 2020.

Stevens, L. A., Nettles, M., Davis, J. L., Creyts, T. T., Kingslake, J., Ahlstrøm, A. P., and Larsen, T. B.: Helheim Glacier diurnal velocity fluctuations driven by surface melt forcing, Journal of Glaciology, 68, 77–89, https://doi.org/10.1017/jog.2021.74, 2022.

Stewart, C. L., Christoffersen, P., Nicholls, K. W., Williams, M. J., and Dowdeswell, J. A.: Basal melting of Ross Ice Shelf from solar heat absorption in an ice-front polynya, Nature Geoscience, 12, 435–440, https://doi.org/10.1038/s41561-019-0356-0, 2019.

Still, H., Campbell, A., and Hulbe, C.: Mechanical analysis of pinning points in the Ross Ice Shelf, Antarctica, Annals of Glaciology, 60, 32–41, https://doi.org/10.1017/aog.2018.31, 2019.

Tétreault, P., Kouba, J., Héroux, P., and Legree, P.: CSRS-PPP: an internet service for GPS user access to the Canadian Spatial Reference Frame, Geomatica, 59, 17–28, 2005.

Thomas, R., Scheuchl, B., Frederick, E., Harpold, R., Martin, C., and Rignot, E.: Continued slowing of the Ross Ice Shelf and thickening of West Antarctic ice streams, Journal of Glaciology, 59, 838–844, https://doi.org/10.3189/2013JoG12J122, 2013.

Thomas, R. H.: Ice shelves: a review, Journal of Glaciology, 24, 273–286, 1979.

Tinto, K. J., Padman, L., Siddoway, C. S., Springer, S. R., Fricker, H. A., Das, I., Caratori Tontini, F., Porter, D. F., Frearson, N. P., Howard, S. L., Siegfried, M. R., Mosbeux, C., Becker, M. K., Bertinato, C., Boghosian, A., Brady, N., Burton, B. L., Chu, W., Cordero, S. I., Dhakal, T., Dong, L., Gustafson, C. D., Keeshin, S., Locke, C., Lockett, A., O'Brien, G., Spergel, J. J., Starke, S. E., Tankersley, M., Wearing, M. G., and Bell, R. E.: Ross Ice Shelf response to climate driven by the tectonic imprint on seafloor bathymetry, Nature Geoscience, 12, 441–449, https://doi.org/10.1038/s41561-019-0370-2, 2019.

965 Trusel, L., Frey, K., Das, S., Karnauskas, K., Munneke, P., Meijgaard, E., and Van den Broeke, M.: Divergent trajectories of Antarctic surface melt under two twenty-first-century climate scenarios, Nature Geoscience, 8, 927–932, https://doi.org/10.1038/ngeo2563, 2015.

Van Der Veen, C. J., Stearns, L. A., Johnson, J., and Csatho, B.: Flow dynamics of Byrd Glacier, East Antarctica, Journal of Glaciology, 60, 1053–1064, 2014.

van der Wel, N., Christoffersen, P., and Bougamont, M.: The influence of subglacial hydrology on the flow of Kamb Ice Stream, West
970 Antarctica, Journal of Geophysical Research: Earth Surface, 118, 97–110, 2013.

Van Wessem, J. M., van de Berg, W. J., Noël, B. P. Y., van Meijgaard, E., Amory, C., Birnbaum, G., Jakobs, C. L., Krüger, K., Lenaerts, J. T. M., Lhermitte, S., Ligtenberg, S. R. M., Medley, B., Reijmer, C. H., van Tricht, K., Trusel, L. D., van Ulft, L. H., Wouters, B., Wuite, J., and van den Broeke, M. R.: Modelling the climate and surface mass balance of polar ice sheets using RACMO2 – Part 2: Antarctica (1979–2016), The Cryosphere, 12, 1479–1498, https://doi.org/10.5194/tc-12-1479-2018, 2018.

975 Vaughan, D. G. and Doake, C.: Recent atmospheric warming and retreat of ice shelves on the Antarctic Peninsula, Nature, 379, 328–331, 1996.

Whillans, I., Chen, Y., Van Der Veen, C. J., and Hughes, T.: Force budget: III. Application to three-dimensional flow of Byrd Glacier, Antarctica, Journal of Glaciology, 35, 68–80, 1989.

Whiteford, A., Horgan, H., Leong, W., and Forbes, M.: Melting and refreezing in an ice shelf basal channel at the grounding line of the Kamb
980 Ice Stream, West Antarctica, Journal of Geophysical Research: Earth Surface, 127, e2021JF006 532, 2022.

Zou, X., Bromwich, D. H., Montenegro, A., Wang, S.-H., and Bai, L.: Major surface melting over the Ross Ice Shelf part I: Foehn effect, Quarterly Journal of the Royal Meteorological Society, 147, 2874–2894, 2021a.

Zou, X., Bromwich, D. H., Montenegro, A., Wang, S.-H., and Bai, L.: Major surface melting over the Ross Ice Shelf part II: Surface energy balance, Quarterly Journal of the Royal Meteorological Society, 147, 2895–2916, 2021b.

985 Zumberge, J., Heflin, M., Jefferson, D., Watkins, M., and Webb, F.: Precise point positioning for the efficient and robust analysis of GPS data from large networks, Journal of geophysical research: solid earth, 102, 5005–5017, 1997.